Quantum Information and Computation, Vol. 12, No. 5&6 (2012) 0502–0534


# DISTRIBUTION OF ENTANGLEMENT IN NETWORKS OF BI-PARTITE FULL-RANK MIXED STATES

G.J. LAPEYRE, JR.[1], S. PERSEGUERS[2], M. LEWENSTEIN[1,3], A. ACÍN[1,3]

[1] *ICFO–Institut de Ciències Fotòniques*
*Mediterranean Technology Park, 08860 Castelldefels, Spain*

[2] *Max-Planck–Institut für Quantenoptik*
*Hans-Kopfermann-Strasse 1, 85748 Garching, Germany*

[3] *ICREA-Institució Catalana de Recerca i Estudis Avançats*
*Lluis Companys 23, 08010 Barcelona, Spain*

Received September 8, 2011
Revised February 27, 2012

We study quantum entanglement distribution on networks with full-rank bi-partite mixed states linking qubits on nodes. In particular, we use entanglement swapping and purification to partially entangle widely separated nodes. The simplest method consists of performing entanglement swappings along the shortest chain of links connecting the two nodes. However, we show that this method may be improved upon by choosing a protocol with a specific ordering of swappings and purifications. A priori, the design that produces optimal improvement is not clear. However, we parameterize the choices and find that the optimal values depend strongly on the desired measure of improvement. As an initial application, we apply the new improved protocols to the Erdös–Rényi network and obtain results including low density limits and an exact calculation of the average entanglement gained at the critical point.

*Keywords*:

*Communicated by*: I Cirac & G Milburn

## 1 Introduction

The quantum repeater has been at the center of numerous studies addressing the distribution of entanglement over long distances, an essential prerequisite for many tasks in quantum information processing [1, 2]. The central idea of the quantum repeater is to send one of a pair of entangled particles (*e.g.* a photon) across a series of links such that each link is short enough that the probability of absorption is low and then to perform entanglement swappings at each node to further propagate the entanglement. However, the inevitable presence of noise in producing and transporting quantum states renders the straightforward application of repeaters hard in practice. This has resulted in the expenditure of a great deal of effort in designing distribution protocols. While the initial repeater schemes involved a one-dimensional chain of nodes (containing qubits) connected by links, considering higher-dimensional networks of nodes and links has been a fruitful approach because the entanglement in neighboring links

can be concentrated via purification. Given a fixed amount of entanglement per link that can be generated in a particular laboratory setting, this concentration allows a useful amount of entanglement to be distributed over larger distances, which in turn allows protocols that consume entanglement to work over a larger distance. Previous work on entanglement distribution in dimension greater than one considered either pure states [3, 4, 5], or certain mixed states of rank two and three [6, 7]. Pure states were used in previous distribution studies because entanglement is better understood and easier to manipulate in pure states than mixed states. However, realistic noise models imply that a bi-partite system of non-local components may only be prepared in a full-rank mixed state. In fact, it has been shown that long-range entanglement on a cubic lattice of full-rank mixed states is possible [8].

On the other hand, while the bulk of work to date has been concerned with regular lattices, only a few works have treated random networks. The creation of entangled sub-networks on the Erdös–Rényi (ER) model [9] has been studied. Other workers investigated the effect of a particular transformation on several pure–state complex networks as well entanglement swapping with full-rank mixed states on the same networks [10, 11]. These studies showed on one hand that transforming network hubs to rings via LOCC can enhance entanglement distribution on a variety of pure-state networks and on the other hand how distribution is affected by the interplay between the correlation length and the characteristic length of decay of fidelity under swapping. However, detailed studies of the application of of entanglement distribution protocols using both swapping and purification on complex networks have not yet been done. In the present work we address this deficit by introducing some natural optimization problems in distributing entanglement along paths of full-rank mixed states. We find that the solutions to these problems yield surprisingly non-trivial results. Then, as a first application, we apply entanglement concentration protocols to the ER network. One of our main objectives is to understand when the use of the network connectivity offers an advantage for distributing entanglement between two nodes with respect to the simple protocol in which entanglement is swapped along the shortest path connecting them. Note that this is always the case for a classical network: connectivity always helps in distributing classical information through a network. However, this may not be the case in the quantum regime, as quantum information cannot be cloned [12]. Indeed, we provide instances where the simplest direct protocol is better than the considered protocols using the network connectivity.

In Sec. 2, we give an overview of the models that we will examine. We shall consider the average concurrence on networks in which each link is initially a full-rank mixed state on two two-level systems, while a node is a local collection consisting of one party from each link terminating at that node. (See Fig. 1.) Unless stated explicitly, when we speak of average concurrence we mean an average over both the outcomes of quantum measurements and the distribution of links for a given random network. We shall furthermore consider only two quantum operations for distributing entanglement (See Fig. 2.):

- entanglement swapping, which probabilistically replaces a series of two links by a single link that bypasses the common node. The output link is in general less entangled than the input links.

- purification, which essentially replaces two parallel links (*i.e.* sharing the same two nodes) by a single link that is more highly entangled than either input link.

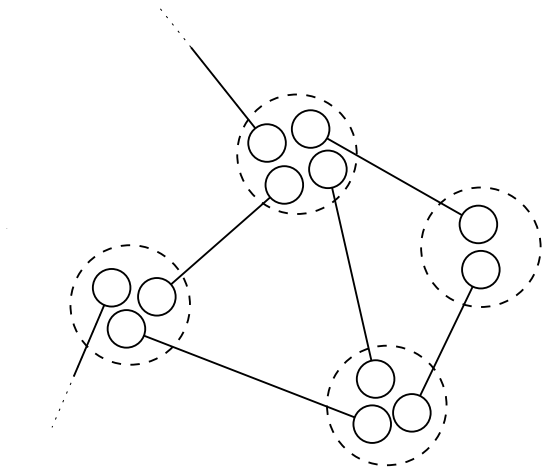

Fig. 1. Part of a quantum network in its initial state. Small circles are qubits. Solid lines are bipartite states. Dashed circles enclose qubits within a node. Local operations may act on all qubits within a node.

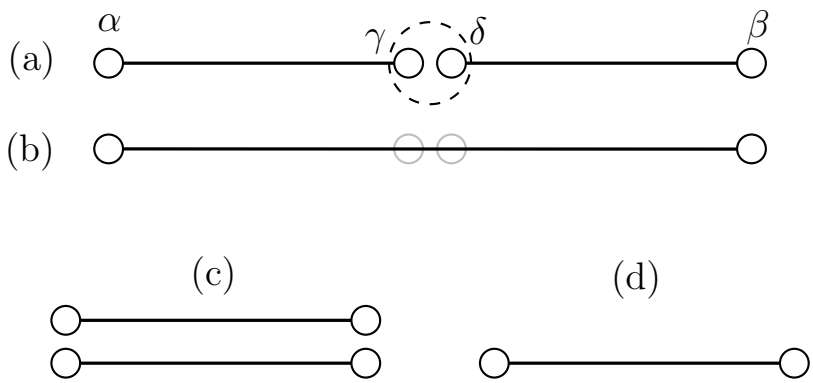


Fig. 2. Entanglement swapping: (a) Before swapping $\alpha$ and $\gamma$ are entangled and $\delta$ and $\beta$ are entangled, but systems $\alpha\gamma$ and $\delta\beta$ are in a product state. (b) After swapping, systems $\alpha$ and $\beta$ are entangled, while $\alpha\beta$ and $\gamma\delta$ are in a product state. Purification: (c) Before purification, two entangled pairs (links). (d) after purification, one pair of nodes has higher entanglement than either of the original pairs.

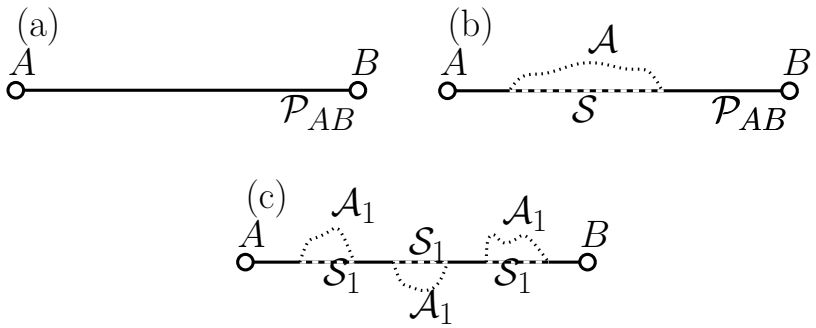


Fig. 3. Establishing entanglement between nodes $A$ and $B$. (a) The shortest path $\mathcal{P}_{AB}$ between $A$ and $B$; the geometry of the path is irrelevant, so we represent it by a straight line with individual links not shown. Other paths connecting $A$ and $B$ are not shown. (b) The shortest path $\mathcal{P}_{AB}$ (solid line with a dashed segment) between $A$ and $B$. Between the endpoints of subpath $\mathcal{S}$ (dashed segment) there is an alternate path $\mathcal{A}$ (dotted line). (c) Similar to (b) with three subpaths and corresponding alternate paths.

The main reason for the restriction to two operations is that many techniques that are successful on pure states, such as multi-partite techniques [13], are difficult, at best, to translate to networks of mixed states. However, these two operations naturally give rise to a rich set of protocols whose design is determined by the quantities that are to be optimized.

In Sections 2, 3, and 4, rather than designing a network for a particular task, we accept a given network of mixed states as a constraint. Our goal is then to identify and solve questions of design that arise in creating protocols to accomplish entanglement distribution. The main question is: *when presented with the option either to swap or to purify, which is the better choice?* For instance:

- *Single purification protocol.* Consider the scenario in Fig. 3b in which we want to entangle nodes $A$ and $B$ using the shortest connecting path $\mathcal{P}_{AB}$ while making use of a neighboring path $\mathcal{A}$. We proceed by swapping at all nodes on the two paths $\mathcal{S}$ and $\mathcal{A}$ to replace each of them by a single link, then purifying these two links, followed by performing swappings on all remaining nodes. In Sec. 4.3 we compute the ratio of path lengths $|\mathcal{S}|/|\mathcal{P}_{AB}|$ that produces the largest average entanglement between $A$ and $B$, finding a value of approximately 0.37.

- If the goal in the previous example is instead to achieve a positive probability of entangling $A$ and $B$ with minimal entanglement per link, then the optimal ratio of path lengths takes the value $1 + \ln 2/\ln([\sqrt{5}-1]/4) \approx 0.409$.

- Consider the scenario shown in Fig. 3c, which we call the *multiple purification protocol*. Here, instead of purifying a single pair of subpaths, we purify $n$ pairs. In Sec 4.4 we compute the minimum entanglement per link required to entangle $A$ and $B$ in the limit of large $n$ for this protocol.

In Sec. 3 we define specifically the direct and quantum strategies mentioned above. In Sec. 4 we analyze the protocols in a more detailed and quantitative way. In Sec. 5 we apply the single purification protocol (SPP) mentioned above to a particular random network— the Erdös–Rényi (ER) network. We present results for short shortest paths and relatively impure

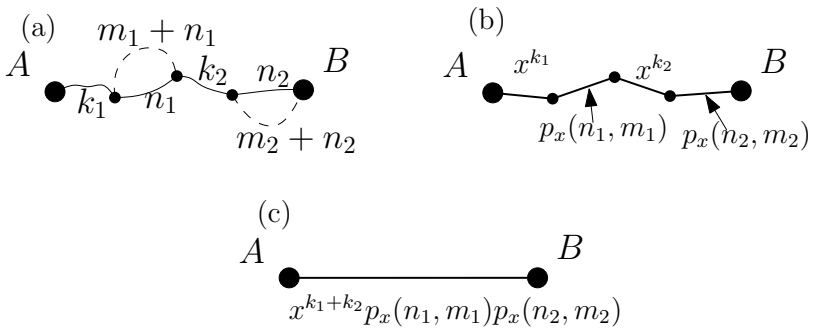


Fig. 4. Quantum protocol. (a),(b), and (c) show the progression of a quantum protocol: (a) Shortest path between $A$ and $B$ $\mathcal{P}_{AB}$ with subpaths of lengths $k_1, k_2, n_1, n_2$. Dotted lines show alternate paths of lengths $m_1 + n_1$ and $m_2 + n_2$. In this paper, we shall always require that the collection of alternative paths and $\mathcal{P}_{AB}$ be mutually disjoint. (b) After swapping and purifying subpaths. Each line segment now represents a single link with the labels giving the resulting Werner parameter. (c) After swapping all links.

states. We also compute the exact asymptotic concurrence of the SPP including all shortest path lengths at the critical point of the model parameter. Finally, is Sec. 6, we address the effects on the protocols of noise in the unitary operations and measurements.

## 2 Elements of the model

We first introduce the networks that we shall consider. We then describe entanglement swapping and purification in more detail.

### *2.1 Network and initial quantum states*

Consider the generic network of nodes and edges shown in Fig 1. With each edge of the network, we associate two two-level systems forming a bipartite system with states on $\mathbb{C}^4$. Thus, each node of degree $k$ is occupied by $k$ qubits. In the following, we shall consider states diagonal in the Bell basis

$$\left\{ |\Phi_{ab}\rangle = \frac{1}{\sqrt{2}} \left( |0a\rangle + (-1)^b |1\bar{a}\rangle \right) : a, b \in \{0, 1\} \right\}.$$

In particular, as the initial state on each edge, we choose the Werner state [14]

$$\rho_W(x) = x |\Phi_{00}\rangle\langle\Phi_{00}| + \frac{1-x}{4} \mathbb{1}_4, \tag{1}$$

which has fidelity $F \stackrel{\text{def}}{=} \langle\Phi_{00}| \rho_W(x) |\Phi_{00}\rangle = (3x+1)/4$. It can be shown that the Werner state is that it is entangled for $x > 1/3$ and separable otherwise. All protocols in this paper attempt to entangle two nodes by creating a Werner state on a pair of qubits, one from each node. Because of its simplicity, the Werner state serves as a standard form, allowing a clearer exposition of the distribution protocols than does a Bell-diagonal state. The Werner state also has the advantage that it is created from any mixed state by removing the off-diagonal elements via a depolarization process, a procedure that can be realized by local operations and classical communication.

### 2.2 Concurrence as a measure of entanglement

In this paper we use concurrence [15] as a measure of useful entanglement in the system. For the Werner state (1) the concurrence is given by

$$C(x) = \max\{0, (3x-1)/2\}. \tag{2}$$

Because our task is to entangle any arbitrarily chosen pair of nodes, we define the average concurrence of the network

$$\bar{C}(x) = \frac{2}{N(N-1)} \sum_{\alpha,\beta} \pi_{\alpha,\beta} C(\alpha,\beta), \tag{3}$$

where $x$ is the parameter of the initial state, $C(\alpha,\beta) = C(x_{\alpha,\beta})$ is the concurrence of the state $x_{\alpha,\beta}$ between $\alpha$ and $\beta$ after applying some protocol, and $\pi_{\alpha,\beta}$ is the probability that this protocol succeeds. Thus this definition depends on the choice of protocol and furthermore assumes that the concurrence of the resulting state between $\alpha$ and $\beta$ is zero with probability $1 - \pi_{\alpha,\beta}$. Note that this average is over both pairs of nodes, as well as probability of the success of the protocol.

In particular, we judge a particular protocol to be better than the direct protocol if it yields a higher concurrence averaged over measurement outcomes. When applied to our protocols on two-qubit Werner states, the concurrence has at least two advantages over other entanglement measures in this respect. Firstly, the concurrence is the unique entanglement measure that is linear in $x$, which makes analysis easier. Secondly, the concurrence provides the extremal comparison in the following sense. Most of the interesting entanglement measures are either convex (for instance, entanglement of formation) or concave (for instance, logarithmic negativity). Suppose that a given protocol has higher average entanglement than the direct protocol if concurrence is used as the measure. In Appendix 1 we show that the protocol also has higher average entanglement, if any convex entanglement measure is used rather than concurrence. Conversely, if the protocol is worse than the direct when judged by concurrence, then it is also worse when judged by any other concave entanglement measure. Finally, we note that for the state (1) the concurrence and the negativity are identical.

### 2.3 Operations for distribution and concentration of entanglement

#### 2.3.1 Entanglement swapping

In this section, we review entanglement swapping, and present the result of applying the operation to Werner states. Consider a state of four qubits $\alpha, \beta, \delta, \gamma$, such that $(\alpha, \gamma)$ is an entangled pair and $(\delta, \beta)$ is an entangled pair, but systems $\alpha\gamma$ and $\delta\beta$ are in a product state. Entanglement swapping is a sequence of quantum operations that transfers entanglement leaving $(\alpha, \beta)$ entangled and $(\delta, \gamma)$ entangled. (See Fig. 2.) In the case of pure states, the optimal swapping is effected by measuring $(\gamma, \delta)$ in the appropriate Bell basis, and then performing a corrective unitary on $\beta$ depending on the outcome of this measurement [16], with the result being either a maximally, or a partially entangled state on $(\alpha, \beta)$. In the latter case, swapping is usually understood to include an attempted singlet conversion on $\alpha\beta$, so that the result of the entire operation is to leave $(\alpha, \beta)$ in either a maximally entangled state (if successful) or a separable state (if unsuccessful.) Mathematically, we consider entanglement swapping to be a map from $\mathbb{C}^4 \otimes \mathbb{C}^4$ to $\mathbb{C}^4$, with the reduction of dimensions resulting from

applying a partial trace over the system $\gamma\delta$. One can show that if the initial states on $(\alpha, \gamma)$ and $(\delta, \beta)$ are both maximally entangled (*eg* Bell states), then the swapping operation succeeds with probability one, assuming perfect operations. In the case of Bell-diagonal mixed states, we cannot know which of the four states we have drawn from the classical ensemble and so cannot unambiguously interpret the result of a measurement. The best we are able do is to assume that we have drawn the most probable state $|\Phi_{00}\rangle$, and proceed with swapping based on this assumption. However, if we have drawn a state other than $|\Phi_{00}\rangle$, we are unfortunately increasing the average classical population of the remaining Bell states. More precisely, given two Bell-diagonal input states whose eigenvalues are $(A, B, C, D)$ and $(A', B', C', D')$, the un-normalized output state after swapping is

$$\begin{aligned}(&AA' + BB' + CC' + DD',\ AB' + BA' + CD' + DC',\\ &AC' + BD' + CA' + DB',\ AD' + BC' + CB' + DA').\end{aligned} \tag{4}$$

Using (1) and (4) it is easy to compute that performing swapping on two Werner states with parameters $x$ and $x'$ produces a Werner state with parameter $xx'$. That is,

$$\rho_W(x) \otimes \rho_W(x') \mapsto\ \rho_W(xx'). \tag{5}$$

*2.3.2 Purification protocol*

Purification protocols operate on a collection of bi-partite mixed states, producing a smaller number of bi-partite states of higher fidelity than the input states [17]. We will use the Bennett-Brassard-Popescu-Schumacher-Smolin-Wootters (BBPSSW) purification protocol, introduced by Bennett *et. al.* [18], which attempts to replace two input Werner states with parameters $x_1$ and $x_2$ by a single, more pure, Werner state— *i.e.* a state with parameter $x'$ satisfying $x' > x_1$ and $x' > x_2$. The parameter of the state resulting from this protocol is

$$x'(x_1, x_2) = \frac{x_1 + x_2 + 4x_1x_2}{3 + 3x_1x_2}, \tag{6}$$

with probability

$$\frac{1 + x_1x_2}{2},$$

while failure results in two separable (*i.e.* useless) states. Usually, in the study of purification protocols, one is concerned with the asymptotic limit of repeated purifications. However, in the present case we are concerned with a single application of (6). One common situation we encounter below is purifying two states with $x_1 = x_2 = x$. Another question is: Given a state $x$, what is the smallest value of $x_{\text{low}} < x$ such that, when the states $x$ and $x_{\text{low}}$ are purified, the result is not worse than both of them; that is $x_{\text{low}}$ for which $x'(x, x_{\text{low}}) = x$. In Fig. 5 we plot $x'(x, x) - x$ and $x - x_{\text{low}}$ *v.s.* $x$. We see that, in order for purification to be useful, $x_1$ and $x_2$ must not be too different, and also that purification is most useful for $x \approx 0.7$–$0.8$; Finally, we note that (6) is increasing in both $x_1$ and $x_2$, a fact that we will use below.

It is well known that the Deutsch-Ekert-Jozsa-Macchiavello-Popescu-Sanpera protocol (DEJMPS), introduced by Deutsch *et. al.* [19], yields states of higher fidelity than the BBPSSW protocol when performing repeated purifications. In fact DEJMPS operates on two generic Bell-diagonal states, producing an output state that is also Bell-diagonal. When applied to two Werner states $\rho_W(x_1)$, and $\rho_W(x_2)$ both protocols yield states with the same

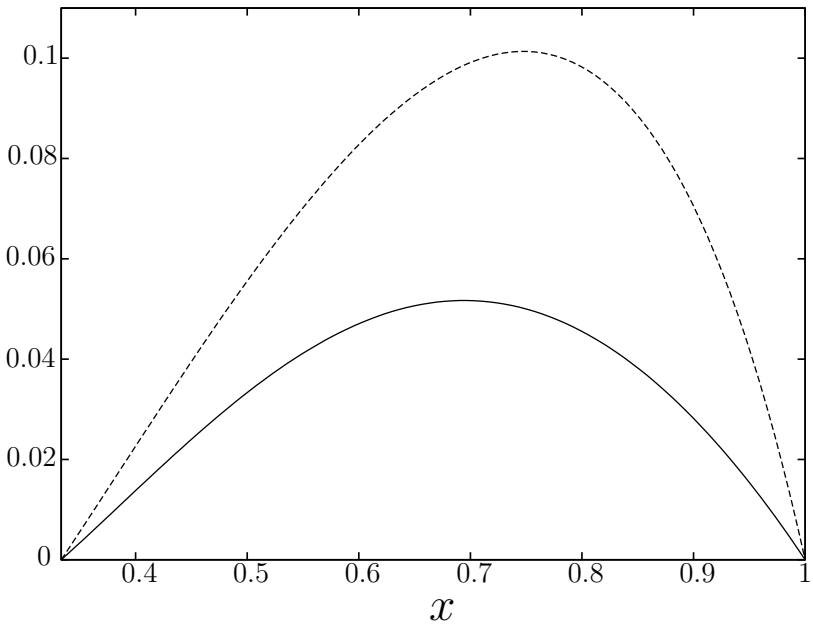


Fig. 5. $x'(x,x)-x$ (solid curve). $x-x_{\text{low}}$, where $x_{\text{low}}$ is determined by $x'(x,x_{\text{low}})=x$. (dashed curve). Both curves cross the $x$-axis at $x=1/3$ and $x=1$.

fidelity and with the same probability of success. However, in general, only the output coefficient of the $|\Phi_{00}\rangle$ component is the same for the two protocols with the remaining three coefficients differing between the protocols. In the case that the two input states are a Werner state and a general Bell-diagonal state with largest eigenvalue $A$, (4) gives a state with concurrence $[(4A-1)x-1]/2$. This result, together with the fact that the swapping (4) is commutative and associative, imply that, for protocols using a single purification, the resulting concurrence is the same whether we use BBPSSW or DEJMPS. On the other hand, direct calculation shows that applying (4) to two states, each of which is the result of purifying two Werner states, yields a state whose concurrence is improved with DEJMPS. In the present work, only the results in Sec. 4.4 are non-optimal in this sense.

Finally, we mention that multiparticle recurrence [20], and hashing [21] protocols have been shown to be more efficient than protocols operating on two copies. Improvements have also been made by optimizing (in part by computer) over a large class of local unitaries [22] rather than using the unitaries employed in BBPSSW and DEJMPS. These protocols may give better results, but they are more opaque conceptually and less amenable to analysis. Furthermore, the gains shown in other contexts are rather modest. Thus, we do not consider these more complicated protocols here.

## 3 Entanglement distribution protocols

### *3.1 Direct strategy*

Our task is to entangle qubits on two selected nodes $A, B$ of the network. The most naive approach is inspired directly by the quantum relay: perform repeated entanglement swappings along the chain of links in the shortest path $\mathcal{P}_{AB}$ connecting $A$ and $B$ using the proce-

dure summarized in (5). (See Fig. 3a.) For instance, swapping the first two links replaces $\rho_{1,2} = \rho_{2,3} = \rho_W(x)$ with one new link $\rho_{1,3} = \rho_W(x^2)$. We then swap the resulting link $\rho_{1,3}$ with $\rho_{3,4} = \rho_W(x)$, yielding $\rho_{1,4} = \rho_W(x^3)$, and so on. Thus, after swapping along the $n$ interior nodes in $\mathcal{P}_{AB}$ we obtain $\rho_{AB} = \rho_W(x^n)$. We call this scheme the direct strategy. It is somehow analogous to a classical problem of transmission on a noisy network with transmission probability $x$ on each link. However, the analogy is not perfect because the classical transmission probability between $A$ and $B$ $x^n$ is in principle useful for any $x > 0$, whereas in our quantum network any Werner state with $x < 1/3$ is separable and thus useless as a resource for quantum information tasks. The concurrence of this direct strategy on a path of $L$ links connecting nodes $\alpha$ and $\beta$ is

$$C^{\text{Direct}}(\alpha, \beta) \stackrel{\text{def}}{=} C(x^L),$$

using $C$ defined in (2).

### *3.2 Quantum strategies*

We may improve on the direct approach by using quantum mechanical operations to concentrate entanglement on the shortest path $\mathcal{P}_{AB}$ connecting $A$ and $B$. In particular, we employ purification schemes to transfer entanglement from neighboring paths to subpaths of $\mathcal{P}_{AB}$. This follows the general idea of concentrating entanglement along a "backbone" that we used in previous work [4]. But, in the present setting, we must introduce new techniques because we are not trying to generate Bell pairs, and we must treat random neighborhoods of the backbone. In what follows, these more complex strategies that exploit the network connectivity are called quantum, although it is clear that the direct protocol is also quantum.

#### *3.2.1 Swapping and purifying*

We begin by presenting the elementary combination of the purification and swapping protocols described above that we shall use in all of the protocols appearing below. Consider two paths, one of $n$ links and the other of $m + n$ links, with identical Werner states $\rho_W(x)$ on each link, for instance, paths $\mathcal{S}$ and $\mathcal{A}$ in Fig. 3b. We first perform entanglement swappings on each chain resulting in two states $\rho_W(x^n)$ and $\rho_W(x^{m+n})$ which share the nodes at their endpoints. We then purify these two states to obtain a Werner state with parameter given by

$$p_x(n, m) = \frac{x^n + x^{m+n} + 4x^{2n+m}}{3 + 3x^{2n+m}}, \tag{7}$$

the operation succeeding with probability

$$\pi_x(n, m) = \frac{1 + x^{2n+m}}{2}. \tag{8}$$

It is not difficult to prove that (7) only yields an improvement over swapping alone (*i.e.* $p_x(n, m) > x_n$) if $m < n$.

#### *3.2.2 Quantum strategy*

Here we present the class of protocols that we study in the remainder of the paper. In subsequent sections, we will study particular cases of this class of strategies. These strategies

yield a higher average concurrence than the direct strategy. Referring to Fig. 3a, we say **subpath** for the segment $\mathcal{S}$ of $\mathcal{P}_{AB}$ that we will purify. We say **alternate path** for a path $\mathcal{A}$ disjoint from $\mathcal{P}_{AB}$ that we use to purify the subpath $\mathcal{S}$. To entangle a pair of nodes $A$ and $B$, the protocol is as follows. (See Fig. 4.)

1. Identify the shortest path $\mathcal{P}_{AB}$ between $A$ and $B$ of length $L$. Or, if there is more than one shortest path, choose one of them.

2. Identify a subpath $\mathcal{S}_1$ of $\mathcal{P}_{AB}$ with end nodes $a_1$, $b_1$ and length $n_1$, such that there is an alternate path $\mathcal{A}_1$ of length $m_1+n_1$ with $0 < m_1 < n_1$ joining $a_1$, $b_1$ that is edge-disjoint with $\mathcal{P}_{AB}$. Note that we cannot have $m_1 < 0$, because this would imply, contrary to our assumption, that $\mathcal{P}_{AB}$ is not a shortest path.

3. Repeat step 2 zero or more times, as shown in Fig. 3c, finding subpaths of lengths $n_i$ and $m_i + n_i$ edge-disjoint from all previously identified paths. As depicted in Fig. 4(b), we now have a collection of subpaths of lengths $n_i$ and $m_i + n_i$ together with subpaths of $\mathcal{P}_{AB}$ for which there is no sufficiently short alternate path.

4. Perform entanglement swapping at each interior node on each of $\mathcal{S}_i$ and $\mathcal{A}_i$, effectively replacing each path of length $l$ with a single Werner state $\rho_W(x^l)$.

5. Purify each pair of states that resulted from a swapping on each pair of paths $(\mathcal{S}_i, \mathcal{A}_i)$, This results in a new path connecting $A$ and $B$ as shown in Fig. 4(c).

6. Swap along the new path connecting $A$ and $B$ to create a new Werner state between $A$ and $B$ with parameter

$$x' = p_x(n_1, m_1)p_x(n_2, m_2)\cdots x^{L-n_1-n_2-\cdots}.$$

In the following discussion, we find it useful to remove the length $L$ from all quantities with the following change of variables.

$$y = x^L, \quad a_i = \frac{n_i}{L}, \quad b_i = \frac{m_i}{L}. \tag{9}$$

Note that $y, a_i, b_i \in [0, 1]$, and that $a_i$ and $b_i + a_i$ are now the fractional lengths of the subpath and alternate path, respectively. The average concurrence of this quantum protocol is then written

$$C^{\mathrm{QM}}(\alpha, \beta) \stackrel{\mathrm{def}}{=} \prod_i \pi_y(a_i, b_i) C\left(y^{1-\sum_j a_j} \prod_i p_y(a_i, b_i)\right), \tag{10}$$

where $i$ and $j$ index the purifications in some arbitrary order, and we have used (7) and (8).

The choice of subpaths is not specified in the steps above, but is rather determined by the desired outcome. Below, we give explicit conditions on the choice of subpaths for optimizing different quantities: maximum size of interval in initial fidelity for which QM protocol is better; $n$ that gives minimum initial fidelity (minimum $x$) for which QM protocol gives positive concurrence; allowed values $n$ near $L$ for which QM protocol is better; $n$ that yields the highest concurrence for fixed $x$. These protocols can, in principle, be applied to any network.

The basic measure of success of the QM protocol given in steps 1–6 above is that it must give a better average concurrence than the direct approach. In the remainder of the paper we shall often be concerned with the increase in concurrence resulting from using a QM protocol. We denote this increase between nodes $\alpha$ and $\beta$ connected by a shortest path of length $L$ by

$$\begin{aligned}\Delta C(\alpha,\beta) =& C^{\mathrm{QM}}(\alpha,\beta) - C^{\mathrm{Direct}}(\alpha,\beta) \\ =& C^{\mathrm{QM}}(\alpha,\beta) - C(y).\end{aligned} \tag{11}$$

Likewise $\Delta\bar{C}$ is $\Delta C(\alpha,\beta)$ averaged over a network. We call the interval in $x$ for which the protocol is successful in this sense (plus some reasonable criteria) the **good interval**. The good interval is determined by the following criteria.

- Each pair of subpath and alternative path must give an improvement in fidelity after purification. That is,
$$p_y(a_i,b_i) > y^{a_i}, \tag{12}$$
if it succeeds. This requirement is necessary to avoid protocols which are advantageous, but would be even better if this particular purification were omitted.

- For $y < 1/3$, the QM protocol must give a concurrence greater than zero. That is,
$$y^{1-\sum_i a_i} \prod_i p_y(a_i,b_i) > \frac{1}{3}. \tag{13}$$
We call the root of the corresponding equality $y_{\mathrm{l}}^*$.

- For $y > 1/3$, the average concurrence of the quantum protocol must be greater than the concurrence of the direct protocol. That is
$$\Delta C(\alpha,\beta) > 0. \tag{14}$$
We call the root of the corresponding equality $y_{\mathrm{h}}^*$. One can show that (12) and (13) give lower bounds on $y$, while (14) gives an upper bound on $y$. Physically this can be seen as follows. If the quantum protocol gives positive concurrence for some value of $y$, then it will continue to do so for larger values of $y$ (this also follows from the fact that (6) is increasing in both arguments). At the upper bound, the effectiveness of the purification is decreasing with increasing $y$ (as seen in Fig. 5), but the probability of success does not increase fast enough to make up for the decrease in the resulting Werner parameter.

Finally, we note that the case in which the input parameter $y < 1/3$ (that is $x < (1/3)^{1/L}$) is especially interesting. In this case, the QM protocol is not only better on average, but is better in a stronger sense in that $C^{\mathrm{Direct}}$ vanishes for $y < 1/3$.

## 4 Analysis of QM protocols

### *4.1 Generic form of constraints*

In this section, we present the constraints in a form that does not provide additional insight, but is useful for later calculations. The constraints (12),(13), and (14) determining the endpoints of the good interval are each of the form

$$f(y,\{d_i\}) = \sum_j K_j y^{c_{j,0}+\sum_i c_{j,i} d_i} > 0, \tag{15}$$

where $\{d_i\}$ is a relabeling of all of the $a_i$ and $b'_i$, and $K$ and $c_{j,i}$ are some numbers depending on $\{d_i\}$ the particular constraint. We are not interested in the details of this formula, but we use it as a tool for calculating quantities appearing below. The end-points of the good interval are determined by the root, $y^*$ between 0 and 1 of $f(y^*, \{d_i\}) = 0$. The end-point determined by (15) is thus given by

$$x^* = y^{*\frac{1}{L}}.$$

We denote by $\hat{y}$ the root of

$$f(\hat{y}, \{d_i = 0\}) = 0. \tag{16}$$

The last expression is useful for computing perturbations around the solution of equations of constraint that are formulated such that all parameters vanish.

### *4.2 Properties of constraints*

These properties hold for all protocols described by the six-step procedure above.

- Consider for the moment just a single subpath of fractional length $a$ and the alternate path of fractional length $a + b$. We ask which is better: swapping along the subpath and ignoring the alternate path, or swapping along each of them and purifying the result. The threshold at which purifying yields a Werner parameter equal to the input is described by $\Delta p_y(a, b) = p_y(a, b) - y^a = 0$, which defines the threshold in each of the parameters $a, b$, and $y$ implicitly as a function of the other two. This equation is easiest to analyze if it is reparameterized as $\Delta p_y(a, ca) = 0$, that is, by eliminating $b$ via $b = ca$. The parameter $c$ is also interesting because it gives the fractional excess length of the alternate path relative to the subpath. It is not difficult to prove that:

  *i*) The threshold $c$ is given by $c = c(y^a)$ where

  $$c(z) = \ln\left(2[1 + 4z - 3z^2]^{-1}\right) \ln^{-1}(z). \tag{17}$$

  *ii*) $c(z)$ takes valid values (*i.e.* non-negative and real) only on $z \in [1/3, 1]$ where we define $c(1)$ by $\lim_{z\to 1} c(z) = 1$.

  *iii*) $c(z)$ increases monotonically in $z = y^a$, so that the threshold $c$ increases(decreases) monotonically in $y$ ($a$).

  *iv*) The difference in Werner parameter $\Delta p_y(a, ca)$ is maximized by $c = 0$ for any fixed $z$, but is maximized by non-trivial $z$ for fixed $c$. For instance, $\Delta p_y(a, 0)$ maximized over $z$ is approximately 0.05 and is given by a root of $3z^4 + 8z^2 - 8z + 1$ with numerical value $z \approx 0.69$.

- Because the map (9) from $y^*$ to $x^*$ is monotonic, the order of end-points of the good interval is preserved as $L$ varies. In fact, the intervals are compressed with increasing $L$. Thus, we only need to analyze the rescaled inequalities.

- The two roots determined by (13) and (14) coincide at $y^* = 1/3$. This is because $C^{\text{Direct}}(y)$ vanishes for $y \leq 1/3$, and increases continuously for $y > 1/3$. Thus $y = 1/3$ is the threshold above which subtracting $C^{\text{Direct}}(y)$ from $C^{\text{QM}}$ is necessary to evaluate whether the QM protocol is useful.

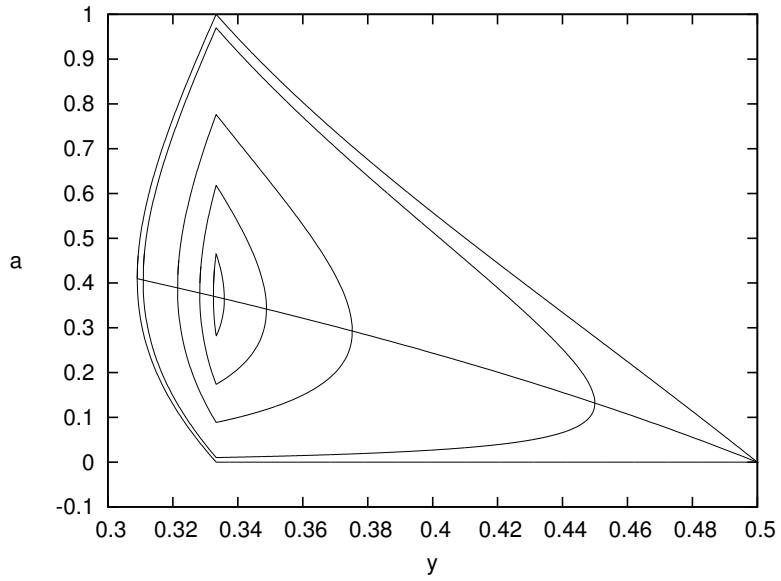


Fig. 6. Roots of $\Delta C_{a,b}^{\mathrm{SPP}}(y) = 0$ from (20) as a function of $y$ and $a$ for various values of $b$. From the outermost to innermost curve the values of $b$ are $0, 0.01, 0.07, 0.11, 0.135$. Curves are determined from closed-form solutions $a = a(y, b)$ with the roots for $b = 0$ in particular given by (21) and (22). The region inside the closed curves is where $\Delta C_{a,b}^{\mathrm{SPP}}(y) > 0$ and thus SPP is advantageous. The curve cutting through the closed curves is $y^a = 2y$ and maximizes $\Delta C_{a,b}^{\mathrm{SPP}}(y)$ with respect to $a$.

- It can be proved that the largest absolute increase $\Delta C$ for the QM protocols compared to the direct, occurs at $y = 1/3$ for all protocols, that is, the largest $y$ for which the direct protocol gives $C^{\mathrm{Direct}} = 0$. This is shown in Fig. 7.

### *4.3 The single purification protocol*

We consider here the case of only a single purification (the single purification protocol [SPP] ) in which we identify only a single subpath and alternative path pair. This situation is shown in Fig. 3b. We analyze the protocol finding optimal values according to the most interesting metrics. In this case there is only one factor in each of the products in (13) and (14), while it is easy to see that (12) is redundant. Then (13) and (14) become

$$y^{1+b} + 4y^{1+a+b} - y^{2a+b} - g(y) > 0, \tag{18}$$

where

$$g(y) = \begin{cases} 1 - y & \text{for } y < 1/3 \\ 5y - 1 & \text{for } y \geq 1/3. \end{cases} \tag{19}$$

In accordance with the discussion above, we require $y, a, b \in (0, 1)$. We call the roots of (18) for $y < 1/3$ and $y \geq 1/3$, $y_{\mathrm{l}}^*$ and $y_{\mathrm{h}}^*$, respectively. Explicitly, the increase in concurrence gained from using SPP is

$$\Delta C_{a,b}^{\mathrm{SPP}}(y) = \frac{1}{4}\left\{y^b\left[4y^2 + y - (y^a - 2y)^2\right] - g(y)\right\}. \tag{20}$$

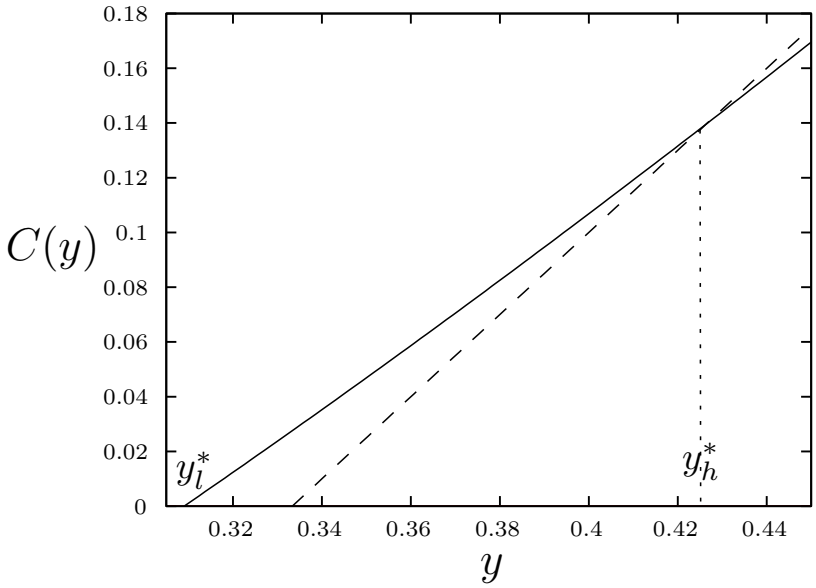


Fig. 7. Average concurrence as a function of scaled Werner parameter $y$. The solid curve is $C^{\rm SPP}_{0.409,0}$ which corresponds to the minimum (at $a = 0.409$) of the leftmost curve for $b = 0$ in Fig. 6. The dashed curve is $C^{\rm Direct}$. Note $\Delta C > 0$ for $y_{\rm l}^* < y < y_{\rm h}^*$. The lower limit $y_{\rm l}^*$ is determined by the largest value of $y$ where $C^{\rm QM} = 0$. The upper limit $y_{\rm h}^*$ is where the curves coincide.

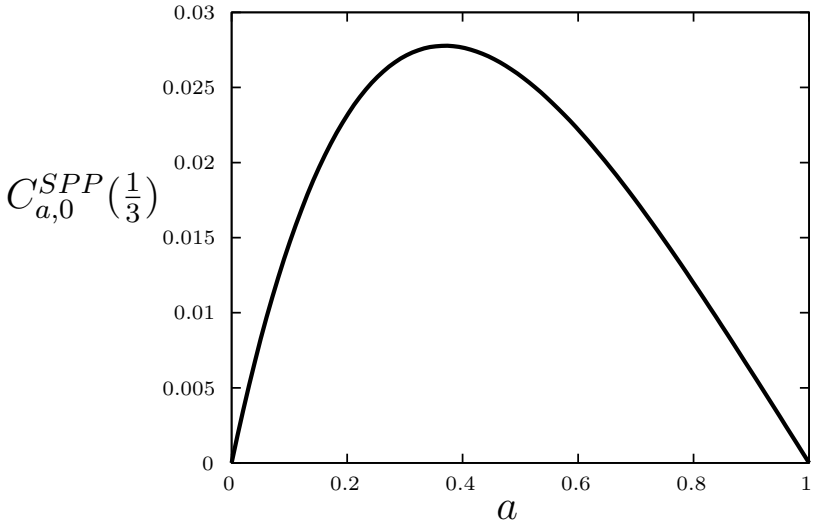


Fig. 8. Concurrence from single purification QM protocol vs. $a = n/L$. For $b = 0$ and $y = 1/3$. This corresponds to the dotted line in Fig. 6. To produce the maximum concurrence, the optimal fractional size of the subpath is $a \approx 0.369$. The curve is generated by setting $b = 0$ in (20), and plotting $C(y = 1/3)$ vs. $a$.

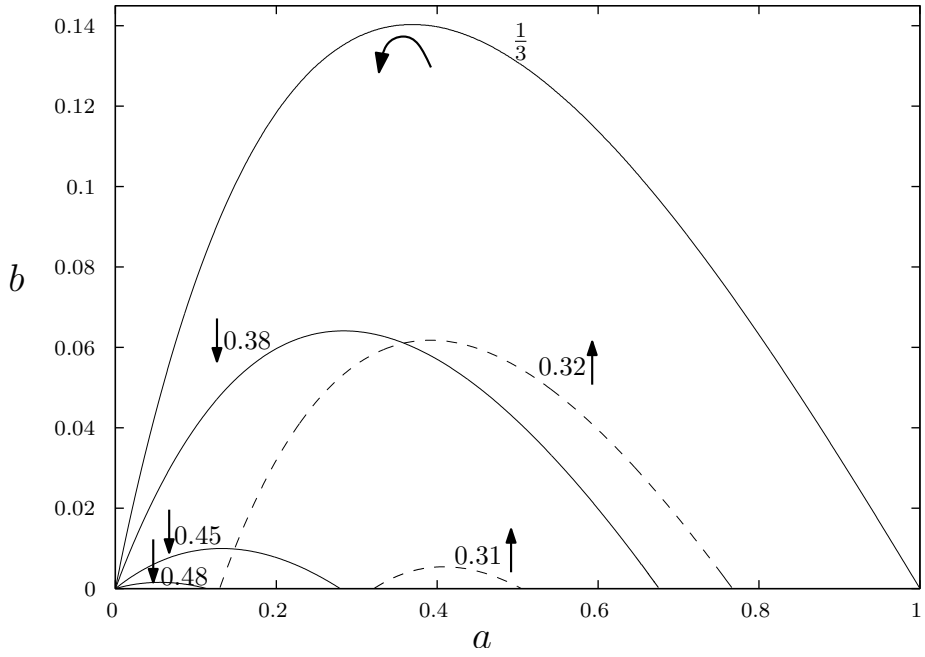


Fig. 9 Region in $ab$-plane for which the single purification QM protocol is better than direct ($\Delta C^{\mathrm{SPP}}_{a,b}(y) > 0$), for several values of $y$. [See (20).] Curves are labeled with corresponding value of $y$. The good area lies below each curve. For $y < 1/3$, curves with increasing $y$ (dashed lines) entirely enclose previous areas. For $y > 1/3$ the same holds for decreasing $y$. The enclosed areas vanish at the smallest $y^*_{\mathrm{l}} \approx 0.309$ and the largest $y^*_{\mathrm{h}} = 1/2$. The curves are determined from closed-form solutions $b = b(y, a)$ of the roots of (20).

Inspecting (20), we see that for fixed $y$ and independently of $b$, $\Delta C_{a,b}^{\mathrm{SPP}}(y)$ is maximized for $a$ solving $(y^a - 2y)^2$. If we further maximize over $b$ and $y$, it is not hard to see that $\Delta C_{a,b}^{\mathrm{SPP}}(y)$ assumes a maximum value of $1/36$ at $b = 0$, $y = 1/3$ and $a = (\log(3) - \log(2))/\log(3)$. To further illustrate the behavior of (20), we consider the simplest case when $a = n/L$, $b = 0$, that is, the shortest path and the alternate path are of the same length. The roots of (20) solved for $a$ are

$$a(y) = 0, \quad a(y) = \frac{\log(4y-1)}{\log(y)}, \tag{21}$$

for $y \geq 1/3$, and

$$a(y) = \frac{\log\left(2y \pm 2\sqrt{\left(y - \frac{\sqrt{5}-1}{4}\right)\left(y + \frac{\sqrt{5}+1}{4}\right)}\right)}{\log(y)}, \tag{22}$$

for $y < 1/3$. In particular, we see that the point where the roots (22) coincide gives the value of $a$ representing the lowest lower bound $y_{\mathrm{l}}^*$ on $y$ and is given by $a = 1 + \ln 2/\ln([\sqrt{5}-1]/4) \approx 0.409$, with (See Fig. 6.)

$$y_{\mathrm{l}}^* = \left(\sqrt{5} - 1\right)/4 \approx 0.309. \tag{23}$$

Thus, this is the optimum value of $a$ to allow the QM protocol to succeed with minimum initial fidelity. On the other hand, the roots (21) coincide at the largest allowed value of $y$,

$$y_{\mathrm{h}}^* = \frac{1}{2}. \tag{24}$$

Inspecting (21) and (22) we also see that the largest good interval in $y$ is obtained for purifying the shortest sub-path, *i.e.* as $a \to 0$. However, the improvement in concurrence also vanishes in this limit. (See Fig. 8). Also note, as shown in Fig. 8, that the value of $a$ that maximizes the concurrence is different from the value that allows minimum initial fidelity as computed above.

We now turn to the case $b \neq 0$ (That is, alternate path is longer than subpath.) Swapping with a single purification is in every way worse than if $b = 0$. This follows from noting that the only effect on SPP of increasing $b$ is to introduce a more weakly entangled state as one of the inputs to the purification. In particular, there is a value of $a = n/L$ above which the QM scheme offers no improvement for any value of $y$. One can further show that the maximum value of $b$ allowing positive $\Delta C_{a,b}^{\mathrm{SPP}}(y)$ is $b = \log(7/6)/\log(3) \approx 0.14$. The region in the $ab$-plane for which the single purification protocol yields an improvement is shown in Fig 9.

### *4.4 Multiple purifications*

Having analyzed the case in which we are allowed a single purification, we now turn our attention to the opposite extreme of unlimited purifications. We partition a fraction $\alpha$ of the shortest path into $n$ subpaths of equal length and purify each subpath with an alternate path of equal length. We ask how this protocol performs as $n \to \infty$ and find that the increase in concurrence tends to a limit, with a lower bound on $y$ for which the protocol is good given by $y = (1/3)^{3/(3-\alpha)}$.

Consider $n$ subpaths $\mathcal{S}_i$ of $\mathcal{P}_{AB}$ of lengths $a_i$, not necessarily covering all of $\mathcal{P}_{AB}$, each of which has a corresponding alternative path $\mathcal{A}_i$ also of length $a_i$ (See Fig 3c.) We first swap

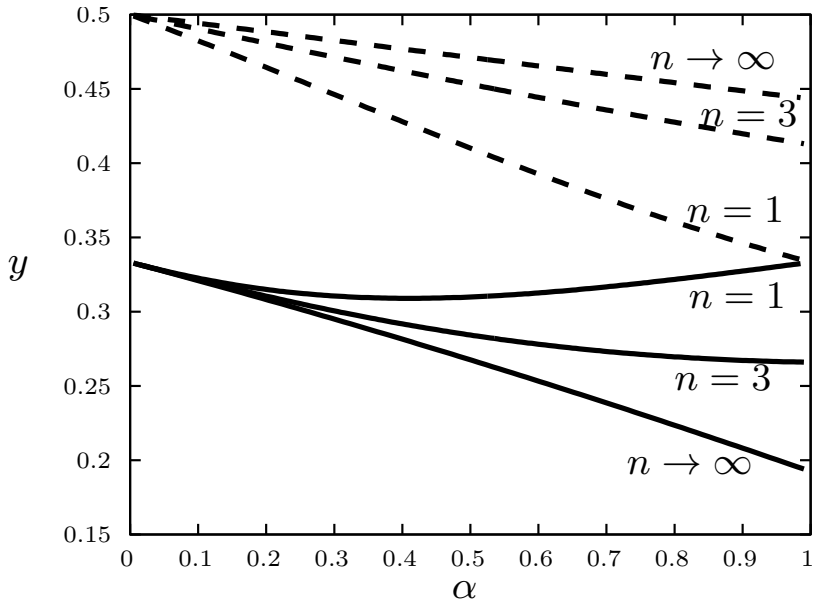


Fig. 10. Constraints on $y$ for multiple purifications with $n = 1, 3, \infty$. The solid curves are $y_{\rm l}^*$. The dashed curves are $y_{\rm h}^*$ from the roots of (26). $y_{\rm l}^*$ for $n \to \infty$ is taken from (25), while all other roots are determined numerically. The values of $y$ between each pair of solid and dotted lines are the good interval, *ie.* those for which the QM scheme is better than direct for the corresponding value of $n$.

along each subpath and alternative path, then purify the resulting pairs. Finally, we swap along the all the remaining internal nodes. In this case we obtain from (13) the inequality for $y_{\rm l}^*$,

$$3\left(\frac{2}{3}\right)^n y\prod_i(1+2y^{a_i}) - \prod_i(1+y^{2a_i}) > 0.$$

Likewise the inequality for $y_{\rm h}^*$ obtained from (14) is

$$\left(\frac{1}{6}\right)^n\left[2^n 3y\prod_i(1+2y^{a_i}) - 3^n\prod_i(1+y^{2a_i})\right] - 3y + 1 > 0$$

In order to investigate the case of purifying many pairs of short paths, we choose the simplest case, setting $a_i = a$ for all $i$ and $a = \alpha/n$. That is, we consider purifications on a fraction $\alpha$ of $\mathcal{P}_{AB}$, in which we purify $n$ pairs of paths, with each path of rescaled length $\alpha/n$. The inequality for $y_{\rm l}^*$ is then

$$3\left(\frac{2}{3}\right)^n y\left(1+2y^{\frac{\alpha}{n}}\right)^n - \left(1+y^{\frac{2\alpha}{n}}\right)^n > 0.$$

The limit of the solution of the corresponding equality as $n \to \infty$ is

$$y_{\rm l}^* = (1/3)^{3/(3-\alpha)}. \tag{25}$$

One can show that the inequality for $y_{\rm h}^*$ as $n \to \infty$ is

$$3y^{\frac{2\alpha}{3}+1} - y^\alpha - 3y + 1 < 0, \tag{26}$$

which we solve numerically. The results are presented in Fig. 10, together with the same curves for a single purification and three purifications. We saw that the value of $\alpha$ giving the minimum possible initial entanglement for a single purification is strictly between 0 and 1. However, for two or more purifications, the minimum is at $\alpha = 1$ (this can easily be proven, as well). Thus, if the goal is for the protocol to work for the smallest possible initial entanglement, then performing purifications along the entire path is best in the present case. Also, both $y_{\mathrm{l}}^*$ and $y_{\mathrm{h}}^*$ decrease with increasing $n$, with the lowest initial entanglement possible giving non-zero concurrence $y = (1/3)^{3/2} \approx 0.19$ for for $\alpha = 1$ and $n \to \infty$. This result demonstrates that for multiple purifications the best protocol performs as many purifications on short subpaths as possible, rather than fewer purifications on longer subpaths. In this sense, purifying before swapping is favorable. It seems very likely that the asymptotic limit mentioned above is the best one can do (with our two allowed operations) without resorting to using previously purified links in further purifications.

### *4.5 Asymptotic form of constraints*

Here we consider the form of the generic inequalities of constraint (15) for large $L$, in order to find simple expressions for the roots, which in turn give the endpoints of the interval where the quantum protocol is advantageous. We must take care, however, because we have some choices when taking this limit. We consider two different classes of limits. The first choice is one in which we ignore the rescaled equations so that $L$ becomes large with $n_i$ fixed. In other words, we are holding the lengths of the subpaths constant as $L$ becomes large. In this case, we find that the leading nontrivial term in the root is of second order in $1/L$. The other choice is to let $L$ become large with $a_i = n_i/L$ constant. In this case, the rescaled equations are unchanged in the large $L$ limit so we only have to look at the asymptotic form of the rescaling $y = x^L$. Thus, for large $L$ with $a_i$ held constant, the roots are given by $x^* \approx 1 + \ln y^*/L$ so that the interval between two constraints decays as $1/L$. That is, the length of the good interval in $x$ decreases as $1/L$,

$$x_2^* - x_1^* \approx \frac{1}{L}(\ln y_2^* - \ln y_1^*).$$

Now we treat the case of holding $n_i$ fixed. We proceed by first taking the small $a_i$ limit of the rescaled equations, followed by the large $L$ limit of the inverse scaling $x = y^{1/L}$. An expansion of the LHS of (15) to first order in both $y$ and $a_i$ gives

$$y^* = \hat{y} - \frac{\sum_i a_i \partial_{a_i} f(\hat{y}, \{\mathbf{0}\})}{\partial_y f(\hat{y}, \{\mathbf{0}\})},$$

where $\hat{y}$ is the root of (16). Replacing $a_i$ by $n_i/L$ and using $(a + b\epsilon)^\epsilon = a^\epsilon + (b/a)\epsilon^2 + O(\epsilon^3)$ we find to second order in $1/L$

$$\begin{aligned} x^* = {y^*}^{\frac{1}{L}} &= \hat{y}^{\frac{1}{L}} - \frac{\sum_i n_i \partial_{a_i} f(\hat{y}, \{\mathbf{0}\})}{L^2 \hat{y} \partial_y f(\hat{y}, \{\mathbf{0}\})} \\ &= \hat{y}^{\frac{1}{L}} - \frac{\ln \hat{y} \sum_j \sum_{i=1} K_j n_i c_{j,i} \hat{y}^{c_{j,0}}}{L^2 \sum_j K_j c_{j,0} \hat{y}^{c_{j,0}}}, \end{aligned} \tag{27}$$

where (15) was used to compute the final line. Before proceeding to examples, we make two remarks on the expansions. *i*) for some values of the parameters $n_i$, the numerator in (27)

vanishes so the that the leading term in $1/L$ in the length of the good interval is of order three. *ii*) In some cases, we want to find the limit (27) for only a subset of $\{a_i\}$, with the others held constant. In this case we simply remove some of the $a_i$ from the sums.

There are several protocols in which these limiting cases are of interest. We mention two of them. Consider for example a network disordered in such a way that most shortest paths have nearly the same length (namely $L$). That is, if the shortest path between A and B is of length $L$, then the available subpaths and alternate paths are most probably of length near $L$. Furthermore, we reconsider the scenario in Sec. 4.3 of a single purification, writing $|\mathcal{S}| = L-q$ and $|\mathcal{A}| = L - r$ with $L$ large and $q$ and $r$ fixed. Thus $q$ and $r$ represent small deviations in the length of available subpaths and alternate paths respectively. In this case, we define $\alpha = q/L$, $\beta = r/L$, and make the substitutions $a = 1 - \alpha$, $b = -\beta$ in (18), and compare the result with (15) taking $\{d_i\} = \{\alpha, \beta\}$ to find the parameters $c_{j,i}$. Applying (27), we find the interval

$$\hat{x} - \frac{\ln 3}{L^2}(3q - 2r) < x < \hat{x} + \frac{\ln 3}{3L^2}(3q - 2r).$$

Thus (assuming the roots are analytic in $1/L$) only for $q/r > 2/3$, does a a good interval exist for large $L$.

In the single and multiple purification schemes above, we saw that the optimal length of the alternate path $\mathcal{A}$ is the same as that of subpath $\mathcal{S}$, that is $m = 0$. However, an alternate path of length exactly $n$ will not be available in general. The lowest order fluctuation in the upper limit of the good interval, as $m$ varies about 0, is studied by examining the small $b$ limit, with the result

$$y^* = \hat{y} + \frac{m \ln \hat{y}(-\hat{y} + 4\hat{y}^{1+a} - \hat{y}^{2a})}{L^2(\hat{y} + 4(1+a)\hat{y}^{1+a} - 2\hat{y}^{2a})}.$$

## 5 Application of Single Purification Protocol to Erdös–Rényi model

We consider the Erdös–Rényi (ER) random graph [23, 24] because it is easier to analyze than more complicated random graphs and gives us insight into the behavior of the purification protocols on more complicated graphs. In particular, we want to compute the average concurrence under the single purification protocol (SPP) of section 4.3 on the ER graph. The ER model is constructed as follows. Begin with the complete graph of $N$ nodes and $N(N-1)/2$ edges and then delete each edge independently with probability $1 - p$. Before proceeding, we simplify the notation below by introducing $m' = n + m$ so that the alternate paths are of length $m'$. In the following, we call $\sigma_L(p)$ the density of shortest paths of length $L$ and $\eta_{L,n,m'}(p)$ the density of SPPs of the given parameters (that is, the fraction of pairs of nodes that admit this SPP). In general there is more than one possible position for the subpath of length $n$ along the SP of length $L$, and $\eta_{L,n,m'}(p)$ includes an average over these positions. The most important results in this section are

- At low bond densities (small $p$) the density of SPPs characterized by $L, n, m'$ is proportional to the product of the densities of shortest paths of length $L$ and length $m'$. That is $\eta_{L,n,m'} \propto \sigma_L \sigma_{m'}$. The constant of proportionality is determined by the number of positions for the subpath.

- At high bond density $\eta_{L,n,m'} \sim \sigma_L$; that is, most subpaths have an available alternate path.

- At the critical point $Np = 1$, and as $N$ increases, all shortest paths are equally likely and the network contains a number of each possible SPP of order 1. As $N$ becomes large and the Werner parameter is near 1, that is, $1 - x$ is small, the concurrence gained by applying all the SPPs is $\Delta\bar{C} \sim AN^{-2}(1-x)^{-4}$ where $A$ is a constant that is easily computed numerically.

As we saw above, the SPP configurations can be partially characterized by the numbers $(L, n, m')$ giving the lengths of the shortest path, the subpath, and the alternate path, respectively. In order to compute the average concurrence for a particular value of Werner parameter $x$, we need to know the densities for various $L, n, m'$ of the shortest paths admitting SPP that are beneficial for this value of $x$. It would greatly simplify understanding the protocol on complex networks if we could write the densities of the SPPs in terms of simpler and better known quantities, such as the distribution of shortest paths. To pursue the connection between these quantities, we compute below the density of all SPPs on the ER network in the small $p$ limit and see that in this limit, the density of an SPP characterized by $L, n, m'$ is proportional to the product of the density of shortest paths of length $L$ and the density of shortest paths of length $m'$. That is, $\eta_{L,n,m'}(p) \approx g(L,n)\sigma_L(p)\sigma_{m'}(p)$. The factor $g$ is discussed below. On the other hand, we argue that, as $p \to 1$, the density of SPPs with fixed $L, n, m'$ is given simply by $\eta_{L,n,m'}(p) \approx \sigma_L(p)$. (That is, nearly all shortest paths admit SPP). Between these two limits densities are more difficult to compute. One might expect similar behavior on other networks that have few connections (small $p$ on the ER network), or many connections (large $p$), but we have not yet studied other networks in detail.

### 5.1 Low Bond Density

In the limit of low bond density $p$, the numbers $L, n, m'$ are enough to compute the density of the corresponding SPP. We take $p$ to be small enough that two or more SPPs are unlikely to be available for a single pair of end point nodes $A$ and $B$. The probability for the SPP configuration is

$$\eta_{L,n,m'}(p) = g(L,n)p^{L+m'}\frac{(N-2)!}{(N-L-m')!} + \mathcal{O}(p^{L+m'+1}), \tag{28}$$

or $\eta_{L,n,m'}(p) \sim g(L,n)p^{L+m'}N^{L+m'-2}$ for large $N$, where

$$g(L,n) = \begin{cases} L-n+1 & \text{for } m' \neq n, \\ (L-n+1)/2 & \text{for } m' = n, \end{cases} \tag{29}$$

is computed in Appendix B. Similarly, we can show

$$\sigma_L(p) = p^L\frac{(N-2)!}{(N-L-1)!} + \mathcal{O}(p^{L+1}),$$

or $\sigma_L(p) \sim p^L N^{L-1}$ for large $N$. It follows that $\eta_{L,n,m'}(p) \sim g(L,n)\sigma_L(p)\sigma_{m'}(p)$ in this limit.

### 5.2 High Bond Density

On the other hand, when $p$ is large enough that a shortest path of length $L$ is rare, then nearly all shortest paths are of length less than $L$. If the SP does not admit an SPP with subpath

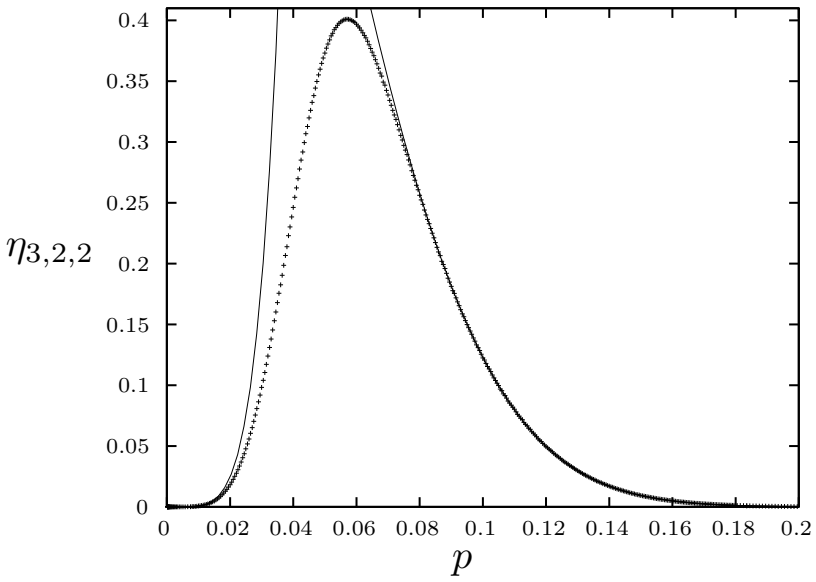


Fig. 11. Density of single path purifications $\eta_{3,2,2}$ for $L = 3, n = 2, m' = 2$, on Erdös–Rényi graph with $N = 200$. Points are MC data. Curve for smaller $p$ is small the $p$ expansion $p^5(N-2)(N-3)(N-4)$. Curve for larger $p$ is the asymptotic formula $(1-p^2)^{N-2}(1-p)$. The small and large $p$ regions are shown in more detail using the same data in Figs. 12 and 13 Error bars are not visible on the scale of the plot.

length $n$, then an edge-disjoint alternate path must be absent in all $L-n+1$ positions, which becomes rare with increasing $p$ and $L$. It follows that nearly all shortest paths of length $L$ will allow an SPP for all possible $n$ and $m'$. Let us consider in particular $L = 3, n = m' = 2$. The density of such SPPs for small $p$ is to lowest order in $p$ $\eta_{3,2,2}(p) = p^5(N-2)(N-3)(N-4)$, as shown in Figs. 11 and 12. For large $p$, the density of this SPP is nearly the density of shortest paths of length 3, which in turn is nearly the probability that the shortest path is not of length 1 or 2. It is easy to show (see Appendix B) that for all $N$ and $p$, $\sigma_1(p) = p$ and $\sigma_2(p) = (1-(1-p^2)^{N-2})(1-p)$. We then have $\eta_{3,2,2} \approx 1-\sigma_2-\sigma_1 = (1-p^2)^{N-2}(1-p)$ for large enough $p$, as shown in Figs. 11 and 13. Thus, as we argued in the beginning of this section, to lowest order in $p$, $\eta_{L,n,m'} \approx \sigma_L \sigma_{m'}$, but this no longer holds for large $p$ where asymptotically $\eta_{L,n,m'} \approx \sigma_L$. Finally, we address the consequences of these observations for the average concurrence. Figure 15 shows the average concurrence as defined in 3 on an ER network as a function of both input Werner parameter $x$ and bond density $p$. This plot illustrates several features of the above analysis. The five concentrations of density correspond to $L = 3, 4, 5, 6, 7$ (larger $L$ were not computed in the MC calculations). For small $p$, longer SPs and SPPs are more prevalent, and these require larger $x$ to be effective. On the other hand, for large enough $p$, most of the SPs are of length 1 and 2, which do not admit SPPs.

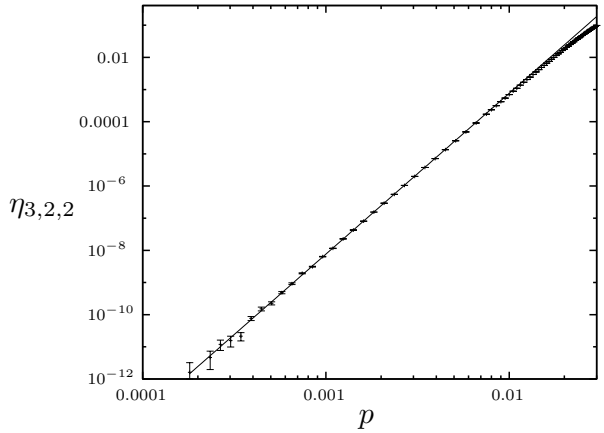


Fig. 12. Density of single path purifications $\eta_{3,2,2}$ for $L = 3, n = 2, m' = 2$, on Erdös–Rényi graph with $N = 200$. Points are MC data (See Appendix D.) Curve is the small $p$ expansion $p^5(N-2)(N-3)(N-4)$.

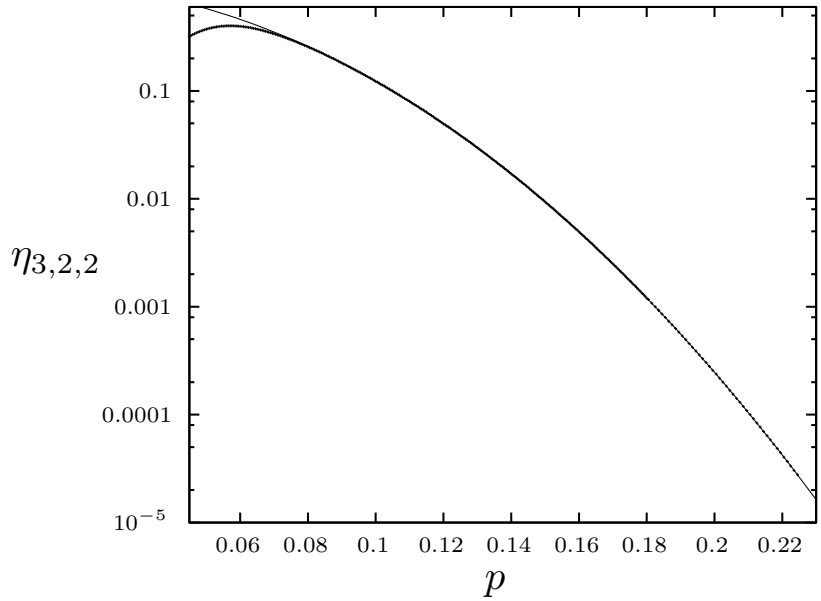


Fig. 13. Density of single path purifications $\eta_{3,2,2}$ for $L = 3, n = 2, m' = 2$, on Erdös–Rényi graph with $N = 200$. Points are MC data. Curve is the asymptotic formula $(1-p^2)^{N-2}(1-p)$. Error bars are not visible on the scale of the plot.

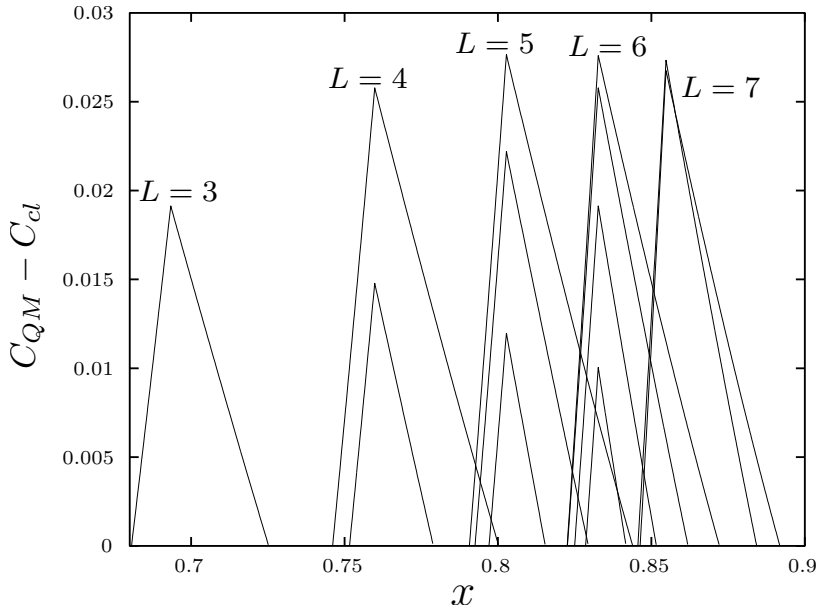


Fig. 14. $\Delta C^{\mathrm{SPP}}_{n/L,m'/L}$ (see (20) given by all possible single purifications with $L \leq 7$, *vs.* the initial Werner parameter $x$. Note that this figure is independent of the structure of the lattice. (Some purifications for $L = 7$ are omitted for clarity.

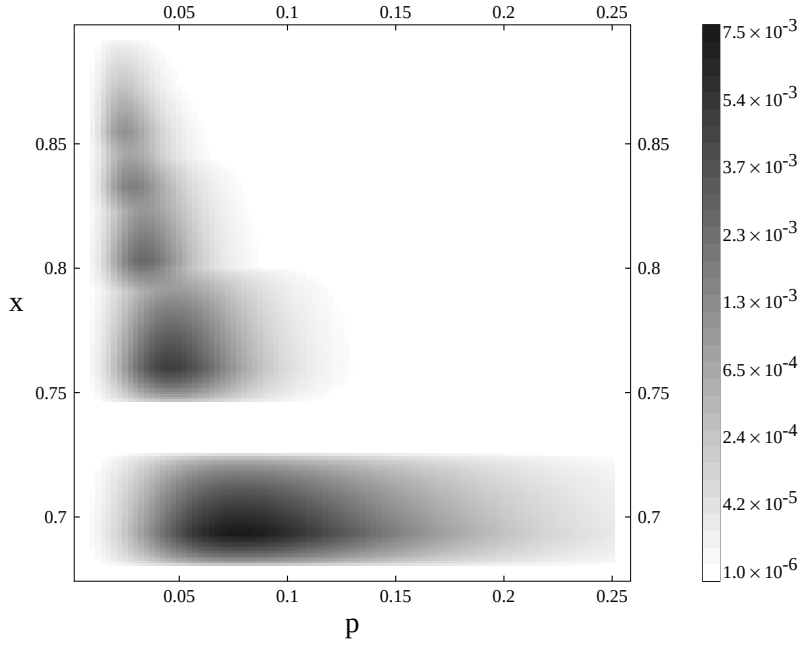


Fig. 15. Gain in concurrence $\Delta\bar{C}$ over the simple method as a function of both $p$ and $x$ on the ER network. Monte Carlo results for $N = 200$, considering all SPPs with $L < 8$.

### 5.3 Concurrence at the critical point $Np = 1$

In this section, we compute the asymptotic average improvement in concurrence $\Delta\bar{C}$ of the critical ER network for $x$ near 1 and large $N$ and find that

$$\Delta\bar{C} \sim \frac{A}{N^2(1-x)^4}. \tag{30}$$

This expression is interpreted as follows. The factor of $N^{-2}$ is the probability that an SPP with any particular $L, n, m$ and position of subpath will occur. The factors of $1/(1-x)$ come from multiple SPPs contributing at one value of $x$: A fixed value of $x$ gets contributions from SPPs with associated SPs of length $L \approx 1/(1-x)$; there are order $L$ such shortest paths; order $L$ different subpaths (of length $n$) for each SP; order $L$ alternate paths for each subpath; order $L$ positions along the shortest path for the subpath.

A few comments on the range of applicability of (30) are in order. In addition to requiring large $N$ and small $1-x$, we require that contributing paths not be too large so that the tree-like approximation remains valid. The most crude bound is that contributing paths be smaller than the radius (largest geodesic) of the network. At the critical point, there is a single cluster of size of order $N^{2/3}$ with all next-largest clusters growing slower than any power. It has been proven recently [25] that the radius of the incipient giant cluster on the critical ER graph grows as $N^{1/3}$ and furthermore (in distinction to the subcritical phase) the smaller clusters have smaller radii. Our numerical simulations show that the the radius of the largest cluster is $aN^{1/3}$, with $a$ approximately equal to 3. Using this radius as a bound on the valid range of $L$ together with $L \approx 1/(1-x)$ in (30), we find that $\Delta\bar{C} < 81AN^{-2/3}$. Thus, we see that the advantage of single-path purification vanishes with increasing $N$ at the critical point of the ER model. We expect similar behavior on other critical models as they will also have a broad distribution of very long paths. On the other hand, if we fix $N = cp^2$, we get asymptotically $\sigma_2 = 1 - \exp(-c)$ and $\sigma_3 = \exp(-c)$, in which case we expect SPP to continue to show an advantage.

The calculation of (30) proceeds as follows. It follows from (28) that

$$\eta_{L,n,m'}(p = 1/N) = g(L,n)p^2 = g(L,n)/N^2 \tag{31}$$

for large $N$. At this value of $p$ the calculation of the average concurrence is simplified in that the contributions from each path admitting SPP have the same dependence on $N$. Figure 14 shows the contributions to $\Delta\bar{C}$ for individual triples $L, n, m'$, each of which is effective over a range of $x$. At $Np = 1$, we are in the low density regime and only one SPP is likely to be present between any pair of vertices. Thus, for any value of $x$, the total contribution at $Np = 1$ is found by summing over the contributions for each triple $L, n, m'$. With increasing $L$, the density of SPPs with nearly the same proportions (that is, $a$ and $b$) increases. Thus, although all these SPPs are equiprobable, as $x$ increases the contributions come from increasingly large $L$ with the number of overlapping ranges increasing without limit as $x \to 1$. In fact, the average concurrence is

$$\Delta\bar{C}(x) \sim \frac{1}{N^2}\int L^3 f(y)\, dL, \tag{32}$$

for large $N$ and $x$ near 1. Here $y = x^L$ and $f(y)$, which accounts for the sum over $n$ and $m'$, is computed in Appendix C. We define $h(s)$ via $h(-\ln(y)) = f(y)$, and use $-\ln x \approx 1 - x = \epsilon$

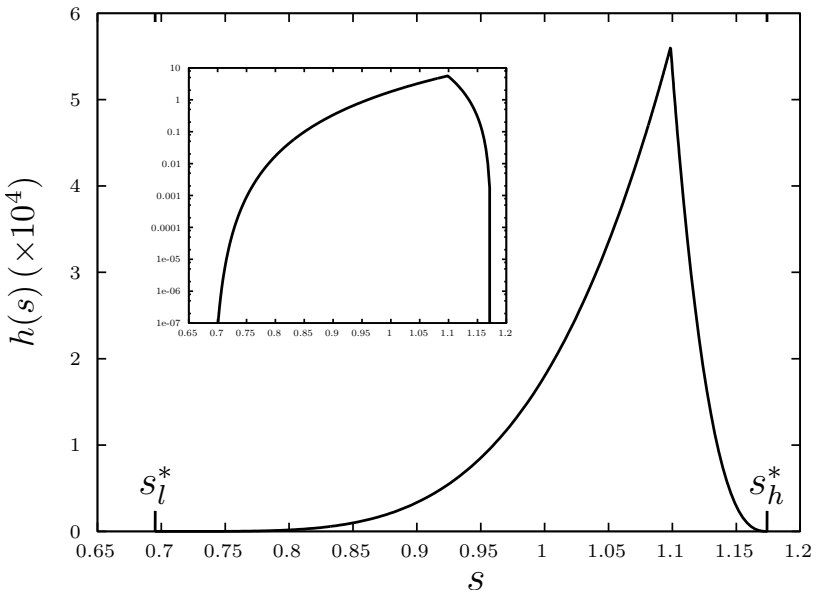


Fig. 16. $h(s)$ appearing in (33). Inset is a semi-log plot of $h(s)$ showing the function vanishing at $s_l^*$ and $s_h^*$ as a power. The curve was determined by numeric integration.

for $x$ near 1. Then integrating (32) over $L$ gives

$$\begin{aligned}\Delta\bar{C}(x) &\sim \frac{1}{N^2}\int L^3 h(\epsilon L)\,dL \\ &= \frac{1}{N^2\epsilon^4}\int_{s_{lo}^*}^{s_{hi}^*} s^3 h(s)\,ds = \frac{A}{N^2\epsilon^4}.\end{aligned} \tag{33}$$

The limits on the integral are determined by the lowest lower bound (23) and largest upper bound (24) on $y$ (as shown in Fig. 6). We have $s_{hi}^* = -\ln(y_{\rm h}^*)$ and $s_{lo}^* = -\ln(y_{\rm l}^*)$ with $A \approx 6.5 \times 10^{-5}$ determined by numeric integration. In Fig. 17 we see that the asymptotic result (33) is approached rapidly with increasing $L$.

## 6 SPP with noisy operations

Until now, we have considered only the ideal case of perfect operations and unlimited resources, with the only noise being that inherent in the Werner state. Even so, the SPP yields only small improvements in concurrence, with a maximum improvement of about 0.03. However, because the maximum concurrence gain from a single successful purifcation using either BBPSSW or DEJMPS is only 0.05, purification schemes typically involve repeated purification of a large number of copies. Thus, the SPP is conceived as a first step to investigate possibilities of entanglement concentration on complex networks and perhaps as a building block in repeated purification schemes. However, noise can prevent even the small improvement in concurrence from a single purifcation so that that further purification is not possible. In this section we briefly consider the effect of imperfect unitaries and measurements on the SPP protocol. We employ a particular noise model for which the effects on the BBPSSW protocol and the swapping protocol were computed in reference [1]. Here, a noisy operation is

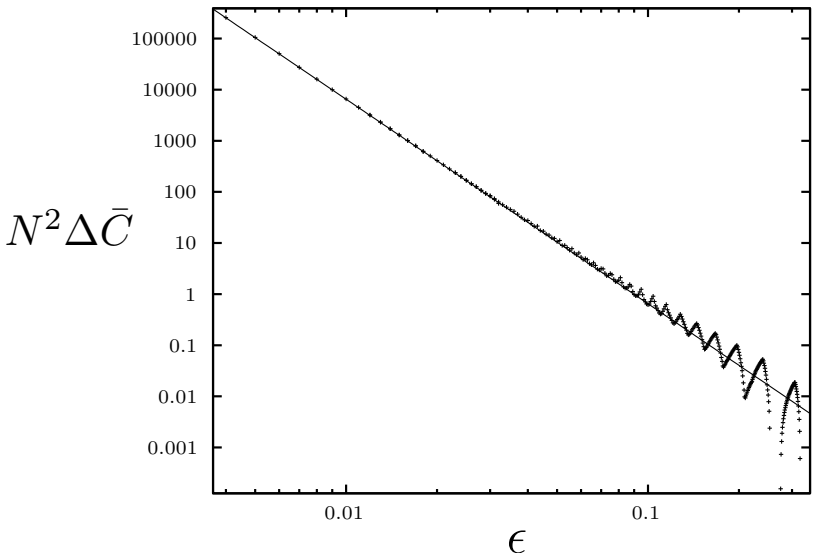


Fig. 17. Average concurrence scaled by $N^2$ *v.s* $\epsilon = 1 - x$ on the ER network with $Np = 1$. The points are computed by summing all contributions of single purifications of shortest paths with $L \leq 300$. The solid line is the asymptotic result $N^2\Delta\bar{C} = A\epsilon^{-4}$. This plot contains no MC, but rather assumes $N$ is large enough that each SPP occurs with the probability given by the low density expansion (31). At the rightmost of the plot are the contributions from the shortest SPP with $L = 3, n = 2, m = 0$.

modeled by a convex combination of the perfect operation and a totally depolarizing channel that acts only on the same subspace as the perfect operation. An two-qubit operation on qubits 1 and 2 with reliability $p_2$ is described by

$$O_{12}\rho = p_2 O_{12}^{\text{ideal}}\rho + \frac{1-p_2}{4}\,\text{tr}_{12}\{\rho\} \otimes \mathbb{1}_{12}, \tag{34}$$

with a similar definition for a single-qubit operator of reliability $p_1$. An imperfect operation on a single qubit with reliability $p_1$ is described in an analagous way. The imperfect measurement in the computational basis of a single-qubit is described by the POVM

$$P_0^\eta = \eta\,|0\rangle\langle 0| + (1-\eta)\,|1\rangle\langle 1| \tag{35}$$

$$P_1^\eta = \eta\,|1\rangle\langle 1| + (1-\eta)\,|0\rangle\langle 0|\,, \tag{36}$$

which is a projective measurement only when the parameter $\eta$ is unity. In [1], the effects of theses noisy operations on each the BBPSSW or DEJMPS and swapping protocols was computed. Although the DEJMPS protocol was reported to be much more robust against noise, it is also much less amenable to analysis and was thus treated numerically. Here, we present simple closed-form results using the BBPSSW protocol. Purification of two input states $\rho_W(x)$ yield a state $\rho_W(x')$ where

$$x' = \frac{(2x + 4x^2)(1-\delta)}{3(1+\alpha) + 3x^2(1-2\delta)}, \tag{37}$$

with $\delta = 2\eta(1-\eta)$ and $\alpha = (1-p_2^2)/p_2^2$. The probability of success is $[1 + \alpha + x^2(1-2\delta)]/2$. It is evident that, when $\alpha = \delta = 0$, these reduce to the result for perfect operations given

by (6). We assume that swapping with noisy operations a chain of $n$ Werner states each of parameter $x$ produces a state

$$x' = \frac{x^n}{c^{n-1}}, \tag{38}$$

with parameter $c \geq 1$, which allows us to track separately the effects of noise from swapping and purification. If we further assume that the error model for unitaries and measurements described above applies to swapping as well, then reference [1] gives

$$c = \frac{3}{p_1 p_2 (4\eta^2 - 1)}. \tag{39}$$

The rescaled Werner parameter for a geodesic of length $L$ is now

$$y = \left(\frac{x}{c}\right)^L.$$

Note that $y$ must now satisfy $y < (1/c)^L$ rather than $y < 1$ as in the case of perfect operations. For simplicity, we restrict our attention to the case $b = 0$ in which the alternate path has optimal length. The average concurrence (11) with noisy swapping and purification is then

$$\begin{aligned} \Delta C_a^{\mathrm{SPP}}(y) = & \frac{1}{4}\Bigg\{ \frac{4c^2(1-\delta)^2}{1-2\delta} y^2 - \tilde{g}(cy) - 2c\delta y \\ & -\alpha - c^2(1-2\delta)\left[y^a - \frac{2(1-\delta)}{1-2\delta} y\right]^2 \Bigg\}, \end{aligned} \tag{40}$$

where

$$\tilde{g}(w) = \begin{cases} 1-w & \text{for } w \leq 1/3 \\ 4w-1 & \text{for } w > 1/3. \end{cases} \tag{41}$$

To simplify the analysis further, we note that for fixed $y$, $\Delta C_a^{\mathrm{SPP}}(y)$ obtains its maximum value at $a = a_{\max}(y)$ for which the squared expression containing $y^a$ in (40) vanishes. Furthermore, the maximum over $y$ is obtained for $y = y_{\max} = 1/(3c)$. This maximum average concurrence

$$\Delta C_{\max}^{\mathrm{SPP}} = \frac{1}{4}\left\{ \frac{4(1-\delta)^2}{9(1-2\delta)} - \frac{1}{3}(1+2\delta) - \alpha \right\}, \tag{42}$$

which is independent of $c$, is plotted in Fig. 18 *v.s.* $p_2$ and $\eta$, normalized to the value for perfect operations 1/36. We see that at $y = y_{\max}$ and $a = a_{\max}(y_{\max})$ for errors of a couple percent, SSP yields improvements of the same order as for perfect operations. This is consistent with the sensitivity of the BBPSSW protocol to noise. In fact, for $y = y_{\max}$ and $a = a_{\max}(y_{\max})$ the values of the noise parameters for which $\Delta C_a^{\mathrm{SPP}}(y)$ vanishes are exactly those for which $x = x'$ in (37).

## 7 Conclusion

We have introduced and solved optimization problems resulting from the interplay between entanglement distribution and concentration. Already for simple protocols, the optimal choice of parameters is non-trivial and depends strongly on the quantity to be optimized.

There are many unexplored questions still to be addressed. For instance, our approach deals with a static initial network and searches for a protocol with no consideration of dynamics.

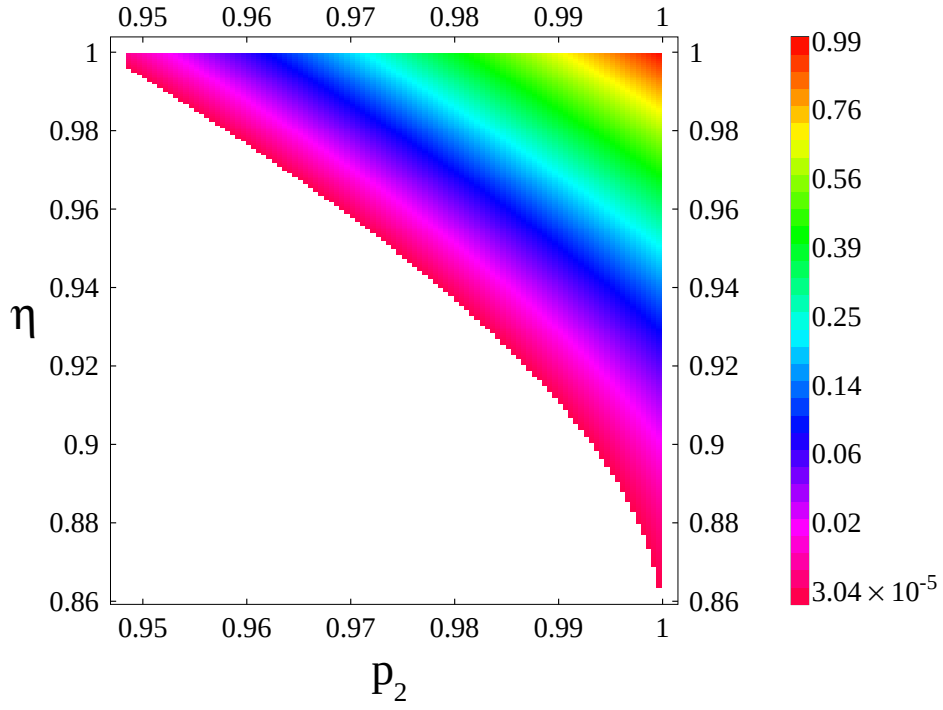


Fig. 18. Maximum value of $\Delta\bar{C}$ with noisy operations, as a function of $p_2$ and $\eta$, normalized to 1 for perfect operations.

**Acknowledgments**

We acknowledge support from ERC grants QUAGATUA and PERCENT, EU projects AQUTE, Q-Essence, NAMEQUAM, Spanish MINCIN FIS-2010-14830, FIS-2008-00784, Consolider-Ingenio QOIT projects, and the Alexander von Humboldt foundation.

**References**

1. W. Dür, H.-J. Briegel, J. I. Cirac, and P. Zoller, Phys. Rev. A **59**, 169 (1999), arXiv:quant-ph/9808065v1.
2. H.-J. Briegel, W. Dür, J. I. Cirac, and P. Zoller, Phys. Rev. Lett. **81**, 5932 (1998), arXiv:quant-ph/9803056v1.
3. A. Acín, J. I. Cirac, and M. Lewenstein, Nature Physics **3**, 256 (2007), arXiv:quant-ph/0612167, URL http://dx.doi.org/10.1038/nphys549.
4. S. Perseguers, J. I. Cirac, A. Acín, M. Lewenstein, and J. Wehr, Phys. Rev. A **77**, 022308 (pages 14) (2008), arXiv:0708.1025, URL http://link.aps.org/abstract/PRA/v77/e022308.
5. G. J. Lapeyre, J. Wehr, and M. Lewenstein, Physical Review A **79**, 042324 (2009), URL http://link.aps.org/doi/10.1103/PhysRevA.79.042324.
6. S. Broadfoot, U. Dorner, and D. Jaksch, EuroPhys. Lett. **88**, 50002 (2009).
7. S. Broadfoot, U. Dorner, and D. Jaksch (2010), arXiv:1008.3584v1.
8. S. Perseguers, Phys. Rev. A **81**, 012310 (2010), arXiv:0910.1459.
9. S. Perseguers, M. Lewenstein, A. Acín, and J. I. Cirac, Nature Physics (2010a), ISSN 1745-2473, URL http://www.mpq.mpg.de/cms/mpq/en/news/press/$10_05_21$.*html*.
10. M. Cuquet and J. Calsamiglia, Phys. Rev. Lett. **103**, 240503 (2009).
11. M. Cuquet and J. Calsamiglia, Phys. Rev. A **83**, 032319 (2011), arXiv:1011.5630, URL http://link.aps.org/doi/10.1103/PhysRevA.83.032319.
12. W. Wootters and W. Zurek, Nature **299**, 802 (1982).
13. S. Perseguers, D. Cavalcanti, G. J. Lapeyre, M. Lewenstein, and A. Acín, Phys. Rev. A **81**, 032327 (2010b), arXiv:0910.2438v1.
14. R. F. Werner, Phys. Rev. A **40**, 4277 (1989).
15. W. K. Wootters, Phys. Rev. Lett. **80**, 2245 (1998), arXiv:quant-ph/9709029v2.
16. S. Bose, V. Vedral, and P. L. Knight, Phys. Rev. A **60**, 194 (1999).
17. W. Dür and H. J. Briegel, Reports on Progress in Physics **70**, 1381 (2007), ISSN 0034-4885, URL http://iopscience.iop.org/0034-4885/70/8/R03;jsessionid=0A1B8144221B414BB2727A1281265614.c2.
18. C. H. Bennett, G. Brassard, S. Popescu, B. Schumacher, J. A. Smolin, and W. K. Wootters, Physical Review Letters **76**, 722 (1996), URL http://link.aps.org/doi/10.1103/PhysRevLett.76.722.
19. D. Deutsch, A. Ekert, R. Jozsa, C. Macchiavello, S. Popescu, and A. Sanpera, Physical Review Letters **77**, 2818 (1996), URL http://link.aps.org/doi/10.1103/PhysRevLett.77.2818.
20. M. Murao, M. B. Plenio, S. Popescu, V. Vedral, and P. L. Knight, Phys. Rev. A **57**, R4075 (1998), arXiv:quant-ph/9712045v1.
21. E. Maneva and J. Smolin, in *Quantum Computation and Quantum Information Science, AMS Contemporary Mathematics Series* (American Mathematical Society, 2002), vol. 305, pp. 203–212, arXiv:quant-ph/0003099v1.
22. J. Dehaene, M. Van den Nest, B. De Moor, and F. Verstraete, Phys. Rev. A **67**, 022310 (2003), arXiv:quant-ph/0207154v1.
23. B. Bollobás, *Random Graphs* (Cambridge University Press, Cambridge, 2006), 2nd ed.
24. R. Durrett, *Random Graph Dynamics* (Cambridge University Press, New York, 2006).
25. A. Nachmias and Y. Peres, Ann. Probab. **36**, 1267 (2008), ISSN 0091-1798, arXiv:math/0701316v4.
26. M. B. Plenio, Phys. Rev. Lett. **95**, 090503 (2005).
27. G. Csardi and T. Nepusz, InterJournal **Complex Systems**, 1695 (2006), URL http://igraph.sf.net.

28. M. Matsumoto and T. Nishimura, ACM Trans. Model. Comput. Simul. **8**, 3 (1998), ISSN 1049-3301, URL `http://doi.acm.org/10.1145/272991.272995`.

## Appendix A Entanglement on two-qubit Werner States

In this appendix we show that the concurrence is the extremal entanglement measure when comparing the quantum to direct protocols. Below, we show that entanglement measures can be parameterize by $C$, *i.e.* $E = E(C)$. We label two values $E_i = E_i(C_i)$ with $i = 1, 2$. The condition (10) has the form

$$pC_2 \geq C_1, \tag{A.1}$$

with $0 < p < 1$. We will show that (A.1) implies $pE_2 \geq E_1$ if and only if $E(C)/C$ is non-decreasing, a condition satisfied by all convex entanglement measures. Thus, if the quantum protocol is advantageous according to concurrence, then it is advantageous according to all convex entanglement measures.

In this paper, an entanglement measure is a function $E$ from density operators to $[0, 1]$ that satisfies the following conditions
*i*) If $\rho$ is separable then $E(\rho) = 0$.
*ii*) $E$(Bell state) $= 1$.

Entanglement measures usually satisfy one or both of two other properties that will not concern us here: LOCC cannot increase the expectation value of the entanglement, and for pure states $E$ reduces to the entropy of entanglement [26]. Many useful entanglement measures are convex, that is,
*iii)* for positive $p_i$ and $\sum_i p_i = 1$,

$$\sum_i p_i E(\rho_i) \geq E\left(\sum_i p_i \rho_i\right).$$

Condition $i$ implies that entanglement measures must vanish for $x \leq 1/3$, so we need not concern ourselves with these states. The concurrence (2) is an invertible linear function for states with $x \geq 1/3$, so they can be parameterize by $C$ rather than $x$, with $C \in [0, 1]$, and we write $E = E(C)$. Because the eigenvalues of the Werner state (1) are linear in $C$, the set of states with $x \geq 1/3$ is closed under convex combinations, so that *iii* implies $E(C)$ is convex. Similar statements can be made about concave functions. We now show that (A.1) implies $pE_2 \geq E_2$ if and only if $E(C)/C$ is non-decreasing. Clearly, (A.1) is equivalent to $p \in [C_1/C_2, 1]$. In the worst case, we must then have $(C_1/C_2)E_2 \geq E_1$, that is, $E(C)/C$ is non-decreasing. That the converse is true can be shown with similar arguments. Furthermore, it is easy to show that for all convex entanglement measures $E(C)/C$ is non-decreasing. A similar argument shows that $pE_2 < E_1$ implies $pC_2 < C_1$ if and only if $E(C)/C$ is non-increasing, a condition that is satisfied by all concave entanglement measures. Finally, it is worth noting that we can make sharper statements. For instance, $E_a(C) = (C + 4C^2 - C^4)/4$ is neither convex nor concave, yet $E_a(C)/C$ is increasing. It can be shown that the inverse of $E_a$, $E_a^{\text{inv}}(C)$, is also an entanglement measure that is neither convex nor concave, but $E_a^{\text{inv}}(C)/C$ is decreasing.

## Appendix B Shortest paths and SPPs on the ER network

In this appendix we compute the density of shortest paths and paths admitting single purification protocol.

*Shortest Paths* The density of shortest paths of length 1 is obviously $\sigma_1(p) = p$. To compute $\sigma_2(p)$, consider the possible path of length 2 between vertices $v_a$ and $v_b$ that passes through $v_c$. This path is absent with probability $1 - p^2$. Note that the collection of paths for each of the $N - 2$ possible $v_c$ together with the possible path of length 1 are mutually edge-disjoint. Thus the probability that there is a path of length 2, but none of length one is $\sigma_2(p) = (1 - (1 - p^2)^{N-2})(1 - p)$. We did not compute $\sigma_3(p)$, which would be more difficult because independence is no longer present. However, we can say something about the case of large and small $p$. For large $p$, $\sigma(p)_{L+1}/\sigma(p)_L$ vanishes with increasing $p$ so that $\sigma_L(p) \approx 1 - \sigma_{L-1}(p) - \sigma_{L-2}(p) \ldots$, which allows us to compute the asymptotic form of $\sigma_3(p)$. On the other hand, for small $p$, the probability of more than one path Between $v_a$ and $v_b$ of length $L$ becomes negligible and $\sigma_L$ is then the sum of the probabilities for each possible SP. The number of ordered choices of intermediate vertices for the SP is $(N-2)(N-3)\ldots(N-L-1)$, each of which corresponds to a path with at least one unique edge. So, for small $p$, $\sigma_L(p) = p^L(N-2)(N-3)\ldots(N-L-1)$. Our Monte Carlo calculations show that this approximation holds for the case $Np = 1$.

*SPPs* The computation of density of SPPs is similar to that of SPs. The number of edges present in an SPP with shortest path of length $L$, subpath of length $n$, and alternate path of length $m'$ is $L+m'$. Likewise the number of intermediate vertices is $L+m'-2$. However, only in the case $n = m'$, the possible permutations of the $L + m' - 2$ vertices can be partitioned into pairs, in which each member of the pair defines an SPP including exactly the same edges. In each pair, the interior vertices of the subpath and the alternate path are swapped, while the remaining vertices are unchanged. This is the origin of the factor of $1/2$ in (29). Finally, the number of ways that the subpath can be placed along a path of length $L$ is $L-n+1$, from which we arrive at (29). Monte Carlo data supporting this expression is shown in Fig. B.1.

## Appendix C Density of contributions to concurrence at the critical point on the ER network

Here we compute $f(y)$ appearing in (32). In the following we let $p = 1/N$. We write $\Delta C_{L,n,m}(x) = \max[C^{\mathrm{QM}}_{L,n,m}(x) - C^{\mathrm{Class.}}_{L,n,m}(x), 0]$ for the average increase in concurrence obtained from purifying an SPP with parameters $L, n, m$ between two vertices. (The average is over quantum outcomes, distribution of ER networks, and possible positions of the subpath.) Here we use $m$ and $m' = n + m$. As above, we have $b = m/L$ which takes values between 0 and 1. Then the contribution to the average increase in concurrence between a pair of vertices for a

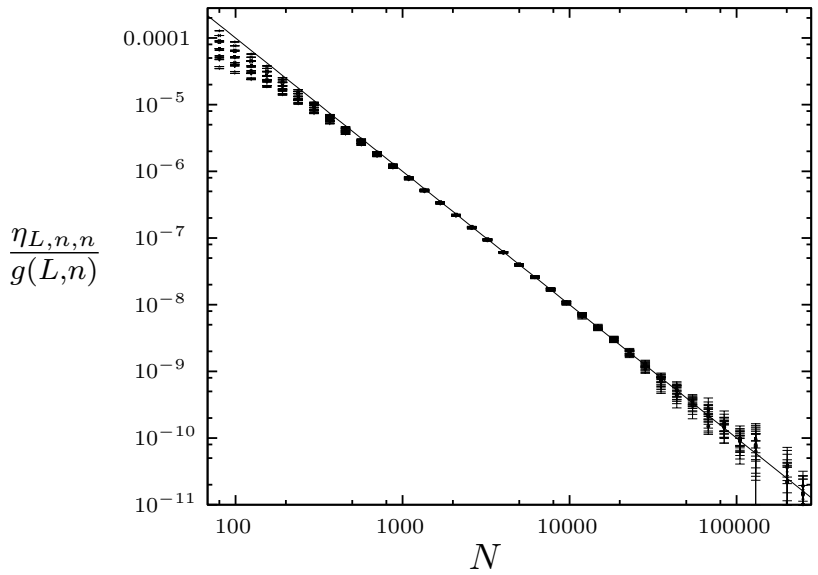


Fig. B.1. $\eta_{L,n,n}/g(L,n)$ *vs.* $N$ at the critical point $Np = 1$ for eleven pairs of $L$ and $n$, from 3,2, through 7,3. The solid line is $N^{-2}$ as predicted by (31). Points are MC data obtained by generating ER network samples and counting the number of SPPs.

fixed value of $L$ is

$$\begin{aligned}
\Delta C_L =& \sum_{n=2}^{L-1}\sum_{m=0}^{n-1} \eta_{L,n,m'}(p)\Delta C_{L,n,m}(x) \\
=& \frac{1}{N^2}\sum_{n=2}^{L-1}\sum_{m=0}^{n-1} g(L,n)\Delta C_{L,n,m}(x) \\
=& \frac{1}{N^2}\sum_{n=0}^{L-1}(L-n+1)\left[\frac{1}{2}\Delta C_{L,n,0}(x)\right. \\
&\left. + \sum_{m=1}^{n-1}\Delta C_{L,n,m}(x)\right] \\
=& \frac{L}{N^2}\sum_{a=2/L}^{1-1/L}(1-a+1/L)\left[\frac{1}{2}\Delta C_{1,a,0}(x)\right. \\
&\left. + \sum_{b=1/L}^{a-1/L}\Delta C_{1,a,b}(x)\right],
\end{aligned}$$

where we used (29), and $a = n/L$, $b = m/L$ take discrete values. This expression holds for large $N$, but for all $x$ and $L$. Now for large $L$ we replace the sum with an integral and find

$$\begin{aligned}\Delta C_L =& \frac{L^2}{N^2}\int_0^1 da\,(1-a)\left[\frac{1}{2}\Delta C_{1,a,0}(x)\right.\\ &\left.+ L\int_0^1 db\,\Delta C_{1,a,b}(x)\right]\\ =& \frac{L^3}{N^2}\int_{0,0}^{1,1}(1-a)\Delta C_{1,a,b}(y)\,da\,db = \frac{L^3}{N^2}f(y).\end{aligned}$$

In the last line, we discarded the term that is of order $L^2$ and kept the term of order $L^3$. The final expression is valid for all $x$, but for any fixed value of $x$, $\Delta C_L$ vanishes with increasing $L$ because $y = x^L$. In practice, we compute $f(y)$ numerically by integrating (10) over values $a$ and $b$ for which $\Delta C$ is positive as shown in Fig 9. The integrand could be done analytically, but the boundaries in Fig 9 are determined via numerical roots in any case.

## Appendix D Monte Carlo computations

We used a modified version of the C language library *igraph* [27] for Monte Carlo calculations. In particular, we replaced the calls to the system random number generator with the Mersenne twister [28] generator. The number of trials for computing statistics varies greatly with model parameters from a few tens to $10^9$. Error bars for quantities such as the number of SPs and SPPs were computed from the sample variance in the mean number of events per network as $\sigma/\sqrt{n_t}$ where $n_t$ is the number of trials. In a few instances, for the largest error bars, $n_t$ is not large and the error bars are thus not accurate.